

A super-smooth C^1 spline space over planar mixed triangle and quadrilateral meshes

Jan Grošelj^{a,b,c}, Mario Kapl^{d,e}, Marjeta Knez^{a,c}, Thomas Takacs^{f,*}, Vito Vitrih^g

^aFMF, University of Ljubljana, Jadranska 19, 1000 Ljubljana, Slovenia

^bAbelium d.o.o., Kajuhova 90, 1000 Ljubljana, Slovenia

^cIMFM, Jadranska 19, 1000 Ljubljana, Slovenia

^dDepartment of Engineering & IT, Carinthia University of Applied Sciences, Europastraße 4, 9524 Villach, Austria

^eRICAM, Austrian Academy of Sciences, Altenberger Str. 69, 4040 Linz, Austria

^fInstitute of Applied Geometry, Johannes Kepler University Linz, Altenberger Str. 69, 4040 Linz, Austria

^gUP FAMNIT and UP IAM, University of Primorska, Glagoljaška 8, 6000 Koper, Slovenia

Abstract

In this paper we introduce a C^1 spline space over mixed meshes composed of triangles and quadrilaterals, suitable for FEM-based or isogeometric analysis. In this context, a mesh is considered to be a partition of a planar polygonal domain into triangles and/or quadrilaterals. The proposed space combines the Argyris triangle, cf. [1], with the C^1 quadrilateral element introduced in [9, 33] for polynomial degrees $p \geq 5$. The space is assumed to be C^2 at all vertices and C^1 across edges, and the splines are uniquely determined by C^2 -data at the vertices, values and normal derivatives at chosen points on the edges, and values at some additional points in the interior of the elements.

The motivation for combining the Argyris triangle element with a recent C^1 quadrilateral construction, inspired by isogeometric analysis, is two-fold: on one hand, the ability to connect triangle and quadrilateral finite elements in a C^1 fashion is non-trivial and of theoretical interest. We provide not only approximation error bounds but also numerical tests verifying the results. On the other hand, the construction facilitates the meshing process by allowing more flexibility while remaining C^1 everywhere. This is for instance relevant when trimming of tensor-product B-splines is performed.

In the presented construction we assume to have (bi)linear element mappings and piecewise polynomial function spaces of arbitrary degree $p \geq 5$. The basis is simple to implement and the obtained results are optimal with respect to the mesh size for L^∞ , L^2 as well as Sobolev norms H^1 and H^2 .

Keywords: C^1 discretization, Argyris triangle, C^1 quadrilateral element, mixed triangle and quadrilateral mesh

1. Introduction

Isogeometric analysis (IGA) was introduced in [23] to apply numerical analysis directly to the B-spline or NURBS representation of CAD models. Since IGA is based on B-spline representations, it is capable to generate smooth discretizations, which are used to discretize higher order PDEs, e.g. [54]. Applications which need higher order smoothness (at least C^1) are, e.g. Kirchhoff–Love shell formulations [35, 36], the Navier–Stokes–Korteweg equation [18], or the Cahn–Hilliard equation [17].

CAD models are composed of several B-spline or NURBS patches, which are smooth in the interior. To obtain higher order smoothness for complicated geometries one has to additionally impose smoothness across

*Corresponding author.

Email addresses: jan.groselj@fmf.uni-lj.si (Jan Grošelj), m.kapl@fh-kaernten.at (Mario Kapl), marjetka.knez@fmf.uni-lj.si (Marjeta Knez), thomas.takacs@jku.at (Thomas Takacs), vito.vitrih@upr.si (Vito Vitrih)

patch interfaces. One possibility is a manifold-like setting, which merges two patches across an interface in a C^k fashion, creating overlapping charts, and remains C^0 near extraordinary vertices, where several patches meet, see [10, 49]. Such approaches need to be modified to increase the smoothness at extraordinary points. One may introduce singularities and define a suitable, locally modified space [41, 42, 56].

These approaches are strongly related to constructions based on subdivision surfaces [46], such as [48, 58] based on Catmull–Clark subdivision over quadrilateral meshes or [14, 26] based on Loop subdivision over triangle meshes.

Smooth function spaces over general quadrilateral meshes for surface design predate IGA, such as [19, 43, 47]. These constructions rely on the concept of geometric continuity, that is, in the case of G^1 , surfaces that are tangent continuous without having a C^1 parametrization. Also before IGA (or around the same time), several approaches were developed for numerical analysis of higher order problems over quad meshes, such as the Bogner–Fox–Schmit element [7], the elements developed by Brenner and Sung [9] for $p \geq 6$, or the constructions in [4, 39]. See Figure 1 for a visualization of the Bogner–Fox–Schmit and Brenner–Sung elements. Recently, a family of C^1 quadrilateral finite elements was described in [33].

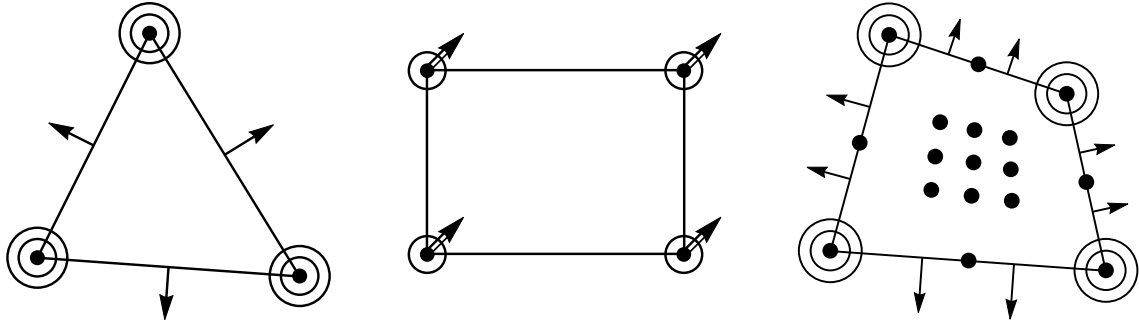


Figure 1: The Argyris element of degree 5 (left), the Bogner–Fox–Schmit element of bi-degree 3 (center) and the Brenner–Sung element of bi-degree 6 (right). Bullets, small circles and large circles denote the interpolation of function values, gradients and Hessians, respectively. A simple arrow denotes the evaluation of a normal derivative and a double stroke arrow denotes the evaluation of the mixed second derivative. Note that the Bogner–Fox–Schmit element is defined only for rectangles, whereas the Brenner–Sung element is defined for any regular quadrilateral.

Due to the increased interest in IGA, the connection between C^1 isoparametric functions and G^1 surfaces was (re)discovered in the IGA context by [15, 20, 34]. As a consequence, C^1 isogeometric spaces over quadrilateral meshes or multi-patch B-spline configurations were studied extensively, see also [5, 6, 11, 27, 29–32, 40].

Already before the introduction of IGA, C^1 splines over triangles were introduced and also used for numerical analysis. The first approach to obtain C^1 discretizations for analysis was the Argyris finite element [1], see also [8, 13] and Figure 1. Other constructions for splines over triangulations followed [16, 21, 57], see also the book [38]. Recently, also due to IGA, there is more interest in splines over triangulations [25, 28, 52, 53].

There are some straightforward connections between splines over triangulations and splines over quadrangulations. Triangular and tensor-product Bézier patches are two alternative generalizations of Bézier curves and are related in the following way. Triangular patches can be interpreted as singular tensor-product patches, where one edge is collapsed to a single point [22, 55].

In this paper we combine the C^1 constructions for triangles and quadrilaterals for degrees $p \geq 5$. We extend the idea of Hermite interpolation with Argyris triangle elements from [24] as well as the framework from [33] for quad meshes to mixed quad-triangle meshes. The approach is similar to the most general setting in [40]. However, we focus on having given a physical mesh instead of a topological one and we provide a construction which is local to the elements.

Such a mixed triangle and quadrilateral mesh can be relevant for many applications. Fluid-structure interaction problems are often solved by combining two different PDE formulations, discretized differently, within a single setup [3]. Combining triangle and quadrilateral patches in a geometrically continuous fashion

is also of relevance for the geometric design of surfaces, see e.g. [44]. Mixed meshes may also arise from trimming [37, 50]. Most CAD software relies on trimming procedures to perform Boolean operations. In that case a B-spline patch is modified by modifying its parameter domain, which is usually a box. The parameter domain is then given as a part of the full box, where some parts are cut out by so-called trimming curves. These trimming curves divide the Bézier (polynomial) elements of the spline patch into inner, outer and cut elements, where the outer elements and outer parts of cut elements are discarded. In that case the resulting mesh is composed mostly of quadrilaterals, with (in general) triangles, quadrilaterals and pentagons as cut elements near the trimming boundary. For practical purposes (e.g. to simplify quadrature) the cut elements are often split into triangles. Thus, this procedure results in a mixed triangle and quadrilateral mesh (see Figure 2). We also want to point out [51], where the authors combine tensor-product volumes as an outer layer with tetrahedral Bézier elements inside the domain, with an extra layer of pyramidal elements in between.

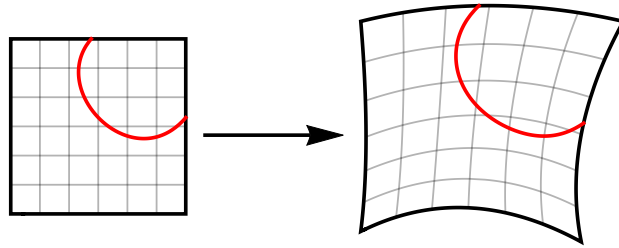


Figure 2: An example of a trimmed patch, where the trimming curve is prescribed in the parameter domain. Note that some of the cut elements are triangles, some are quadrilaterals and some are pentagons.

The paper is organized as follows. In Section 2 we first introduce the notation and mesh configuration which will be used throughout the paper. After that we define the C^1 space over mixed triangle and quadrilateral meshes. Section 3 is devoted to the investigation of continuity conditions across interfaces that need to be considered in the construction of splines from such space. This allows us to analyze properties of the space in Section 4 by introducing and studying a projection operator onto the space. The operator is defined via an interpolation problem and serves us to show that the space is of optimal approximation order. The latter is also verified numerically in Section 5. We present the conclusions and possible extensions in Section 6.

2. The Argyris-like space \mathcal{A}_p

The aim of this section is to introduce necessary notation to describe a domain partition consisting of triangles and quadrilaterals. Over such a mixed mesh we then define a spline space, which can be regarded as an extension of the well-known Argyris space.

2.1. Mixed triangle and quadrilateral meshes

We consider an open and connected domain $\Omega \subset \mathbb{R}^2$, whose closure $\bar{\Omega}$ is the disjoint union of triangular or quadrilateral elements $\Omega^{(i)}$, $i \in \mathcal{I}_\Omega$, edges $\mathcal{E}^{(i)}$, $i \in \mathcal{I}_\mathcal{E}$, and vertices $\mathbf{V}^{(i)}$, $i \in \mathcal{I}_\mathbf{V}$, that is

$$\bar{\Omega} = \left(\dot{\bigcup}_{i \in \mathcal{I}_\Omega} \Omega^{(i)} \right) \dot{\cup} \left(\dot{\bigcup}_{i \in \mathcal{I}_\mathcal{E}} \mathcal{E}^{(i)} \right) \dot{\cup} \left(\dot{\bigcup}_{i \in \mathcal{I}_\mathbf{V}} \mathbf{V}^{(i)} \right), \quad (1)$$

which implies that no hanging vertices exist. Each vertex $\mathbf{V}^{(i)}$ is a point in the plane,

$$\mathbf{V}^{(i)} \in \mathbb{R}^2, \text{ for all } i \in \mathcal{I}_\mathbf{V},$$

and each edge is given by two vertices, i.e.

$$\mathcal{E}^{(i)} = \mathcal{E} \left(\mathbf{V}^{(i_1)}, \mathbf{V}^{(i_2)} \right) = \left\{ (1-v)\mathbf{V}^{(i_1)} + v\mathbf{V}^{(i_2)} : v \in (0, 1) \right\},$$

for all $i \in \mathcal{I}_{\mathcal{E}}$, where $i_1, i_2 \in \mathcal{I}_{\mathbf{V}}$. Each element $\Omega^{(i)}$, with $i \in \mathcal{I}_{\Omega} = \mathcal{I}_{\Delta} \dot{\cup} \mathcal{I}_{\square}$, is either a triangle or a quadrilateral, where \mathcal{I}_{Δ} and \mathcal{I}_{\square} are the sets of indices of the triangle and quadrilateral elements $\Omega^{(i)}$, respectively. We assume that elements are always open sets and use the notation $\Omega^{(i)} = \mathcal{T}(\mathbf{V}^{(i_1)}, \mathbf{V}^{(i_2)}, \mathbf{V}^{(i_3)})$ for triangle elements and $\Omega^{(i)} = \mathcal{Q}(\mathbf{V}^{(i_1)}, \mathbf{V}^{(i_2)}, \mathbf{V}^{(i_3)}, \mathbf{V}^{(i_4)})$ for quadrilateral elements. For all $i \in \mathcal{I}_{\Delta}$ we have

$$\overline{\Omega^{(i)}} = \{(1-u-v)\mathbf{V}^{(i_1)} + u\mathbf{V}^{(i_2)} + v\mathbf{V}^{(i_3)} : (u, v) \in \Delta_0\},$$

where $i_1, i_2, i_3 \in \mathcal{I}_{\mathbf{V}}$ and

$$\Delta_0 := \{(u, v) \in \mathbb{R}^2 : u \in [0, 1], 0 \leq v \leq 1-u\},$$

whereas for all $i \in \mathcal{I}_{\square}$ we have

$$\overline{\Omega^{(i)}} = \{(1-u)(1-v)\mathbf{V}^{(i_1)} + u(1-v)\mathbf{V}^{(i_2)} + uv\mathbf{V}^{(i_3)} + (1-u)v\mathbf{V}^{(i_4)} : (u, v) \in \square_0\},$$

where $i_1, i_2, i_3, i_4 \in \mathcal{I}_{\mathbf{V}}$ and $\square_0 = [0, 1]^2$. We call such a collection of vertices, edges and triangles as well as quadrilateral elements a *mixed triangle and quadrilateral mesh*, or in short a *mixed mesh*.

We denote by $\mathbf{F}^{(i)} : \Delta_0 \rightarrow \overline{\Omega^{(i)}}$, with $i \in \mathcal{I}_{\Delta}$, and $\mathbf{F}^{(i)} : \square_0 \rightarrow \overline{\Omega^{(i)}}$, with $i \in \mathcal{I}_{\square}$, the parametrizations of the elements, which are linear mappings in case of triangles and bilinear in case of quadrilaterals. The parametrizations are always assumed to be regular. An example of a mixed mesh, together with the mappings $\mathbf{F}^{(i)}$, is shown in Fig. 3.

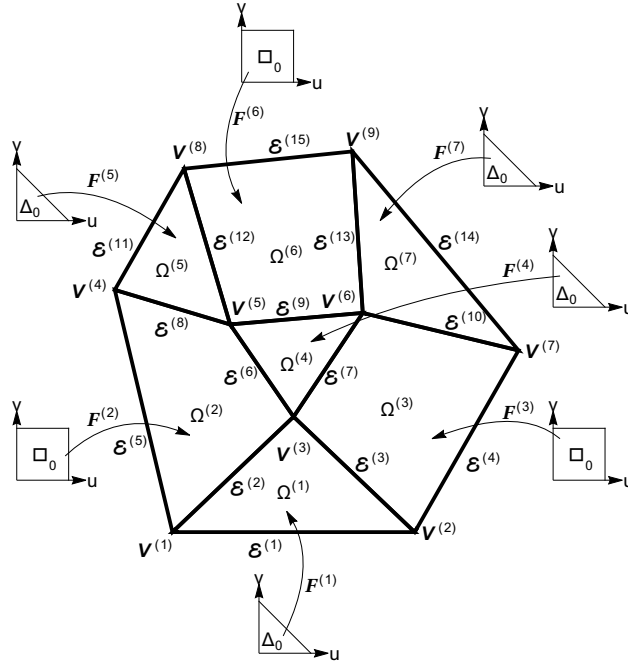


Figure 3: A mixed mesh on a domain Ω consisting of triangular and quadrilateral elements $\Omega^{(i)}$, $i \in \mathcal{I}_{\Omega}$, with edges $\mathcal{E}^{(i)}$, $i \in \mathcal{I}_{\mathcal{E}}$, vertices $\mathbf{V}^{(i)}$, $i \in \mathcal{I}_{\mathbf{V}}$, and the associated geometry mappings $\mathbf{F}^{(i)}$, $i \in \mathcal{I}_{\Omega}$.

2.2. The Argyris-like space \mathcal{A}_p over mixed meshes

Given an integer $p \geq 1$, let \mathbb{P}_p be the space of univariate polynomials of degree p on the unit interval $[0, 1]$, let \mathbb{P}_p^2 denote the space of bivariate polynomials of total degree p on the parameter triangle Δ_0 and let $\mathbb{P}_{p,p}^2$

be the space of bivariate polynomials of bi-degree (p, p) on the unit square \square_0 . We denote by B_i^p , $B_{i,j,k}^{\triangle,p}$ and $B_{i,j}^{p,p}$ the corresponding univariate, triangle and tensor-product Bernstein bases given by

$$B_i^p(u) = \binom{p}{i} u^i (1-u)^{p-i}, \quad i = 0, 1, \dots, p,$$

$$B_{i,j,k}^{\triangle,p}(u, v) = \frac{p!}{i!j!k!} u^i v^j (1-u-v)^k, \quad i, j, k = 0, 1, \dots, p, \quad i+j+k=p,$$

and

$$B_{i,j}^{p,p}(u, v) = B_i^p(u) B_j^p(v), \quad i, j = 0, 1, \dots, p,$$

respectively.

We are interested in the construction and study of a particular super-smooth C^1 spline space of degree $p \geq 5$ on the mixed multi-patch domain Ω defined as

$$\mathcal{A}_p := \left\{ \varphi \in C^1(\overline{\Omega}) : \varphi \circ \mathbf{F}^{(i)} \in \begin{cases} \mathbb{P}_p^2, & i \in \mathcal{I}_{\triangle} \\ \mathbb{P}_{p,p}^2, & i \in \mathcal{I}_{\square} \end{cases}; \varphi \in C^2(\mathbf{V}^{(i)}), i \in \mathcal{I}_{\mathbf{V}}; D_{\mathbf{n}_i} \varphi|_{\mathcal{E}^{(i)}} \in \mathbb{P}_{p-1}, i \in \mathcal{I}_{\mathcal{E}} \right\}. \quad (2)$$

Here $D_{\mathbf{n}_i} \varphi$ denotes the derivative in the direction of the unit vector \mathbf{n}_i orthogonal to the edge $\mathcal{E}^{(i)}$. In what follows, we denote the orthogonal vectors by $(x, y)^\perp := (y, -x)$. In case of a triangle mesh, that is $\mathcal{I}_{\Omega} = \mathcal{I}_{\triangle}$, the space \mathcal{A}_p corresponds to the classical Argyris triangle finite element space of degree p , cf. [1]. Therefore, we refer to the space \mathcal{A}_p as the *(mixed triangle and quadrilateral) Argyris-like space* of degree p . Note that the space \mathcal{A}_p was also discussed in [32] for the case of a quadrilateral mesh (i.e. $\mathcal{I}_{\Omega} = \mathcal{I}_{\square}$) for $p = 5, 6$. Moreover, in [9] the corresponding quadrilateral element was introduced for $p \geq 6$. These constructions were summarized, unified and extended to specific macro-elements for $p = 3, 4$ in [33].

3. Continuity conditions

We study the C^1 continuity conditions relating two neighboring elements from a mixed mesh. After presenting some general results, we devote attention to three specific cases of interest, i.e., a quadrilateral–triangle, triangle–triangle, and quadrilateral–quadrilateral join.

3.1. General conditions across the interface

Without loss of generality let two neighboring elements from the mixed mesh be denoted by $\Omega^{(1)}$ and $\Omega^{(2)}$ and parameterized by (bi)linear geometry mappings

$$\mathbf{F}^{(1)} : \mathcal{D}^{(1)} \rightarrow \overline{\Omega^{(1)}} \quad \text{and} \quad \mathbf{F}^{(2)} : \mathcal{D}^{(2)} \rightarrow \overline{\Omega^{(2)}},$$

where $\mathcal{D}^{(1)}$ and $\mathcal{D}^{(2)}$ denote \square_0 or \triangle_0 . Suppose that $\overline{\Omega^{(1)}}$ and $\overline{\Omega^{(2)}}$ have a common interface $\overline{\mathcal{E}}$ attained at

$$\mathbf{F}^{(1)}(0, v) = \mathbf{F}^{(2)}(0, v), \quad v \in [0, 1]. \quad (3)$$

The graph $\Phi \subset (\overline{\Omega^{(1)}} \cup \overline{\Omega^{(2)}}) \times \mathbb{R}$ of any function

$$\varphi : \overline{\Omega^{(1)}} \cup \overline{\Omega^{(2)}} \rightarrow \mathbb{R}, \quad \varphi(x, y) = \begin{cases} \varphi^{(1)}(x, y), & (x, y) \in \overline{\Omega^{(1)}} \\ \varphi^{(2)}(x, y), & (x, y) \in \overline{\Omega^{(2)}} \setminus \overline{\mathcal{E}} \end{cases}, \quad (4)$$

is composed of two patches given by parameterizations

$$\Phi^{(1)} := \begin{bmatrix} \mathbf{F}^{(1)} \\ f^{(1)} \end{bmatrix} : \mathcal{D}^{(1)} \rightarrow \mathbb{R}^3, \quad \Phi^{(2)} := \begin{bmatrix} \mathbf{F}^{(2)} \\ f^{(2)} \end{bmatrix} : \mathcal{D}^{(2)} \rightarrow \mathbb{R}^3,$$

where $f^{(\ell)} = \varphi^{(\ell)} \circ \mathbf{F}^{(\ell)}$, $\ell = 1, 2$. Along the common interface the function φ is C^1 continuous if and only if its graph Φ is G^1 continuous, i.e.

$$\Phi^{(1)}(0, v) = \Phi^{(2)}(0, v), \quad \det \left[D_u \Phi^{(2)}(0, v), D_u \Phi^{(1)}(0, v), D_v \Phi^{(1)}(0, v) \right] = 0,$$

cf. [15, 20, 34]. Equivalently, it must hold that

$$f^{(1)}(0, v) = f^{(2)}(0, v), \quad (5)$$

$$\alpha_1(v) D_u f^{(2)}(0, v) - \alpha_2(v) D_u f^{(1)}(0, v) + \alpha_3(v) D_v f^{(1)}(0, v) = 0, \quad (6)$$

where

$$\alpha_1(v) := \det \mathbf{J} \mathbf{F}^{(1)}(0, v), \quad \alpha_2(v) := \det \mathbf{J} \mathbf{F}^{(2)}(0, v), \quad \alpha_3(v) := \det \left[D_u \mathbf{F}^{(2)}(0, v), D_u \mathbf{F}^{(1)}(0, v) \right]$$

are the so called *gluing functions* for the interface \mathcal{E} . Note that $\alpha_i(v) \neq 0$ for $v \in [0, 1]$, $i = 1, 2$. The next two lemmas will further be needed. Note that the first one is for the cubic case similar to the construction in [43].

Lemma 1. *For any two bijective and regular C^1 geometry mappings $\mathbf{F}^{(1)}$ and $\mathbf{F}^{(2)}$, such that equation (3) is satisfied, it holds that*

$$\begin{aligned} & \det \mathbf{J} \mathbf{F}^{(2)}(0, v) \left(D_u \mathbf{F}^{(1)}(0, v) \right)^\perp - \det \mathbf{J} \mathbf{F}^{(1)}(0, v) \left(D_u \mathbf{F}^{(2)}(0, v) \right)^\perp = \\ & \det \left[D_u \mathbf{F}^{(2)}(0, v), D_u \mathbf{F}^{(1)}(0, v) \right] \left(D_v \mathbf{F}^{(1)}(0, v) \right)^\perp. \end{aligned} \quad (7)$$

Proof. The result follows from the equalities

$$\det(\mathbf{b}, \mathbf{c}) \mathbf{a} + \det(\mathbf{c}, \mathbf{a}) \mathbf{b} + \det(\mathbf{a}, \mathbf{b}) \mathbf{c} = \mathbf{0}, \quad \det(\mathbf{a}, \mathbf{b}) = \det(\mathbf{a}^\perp, \mathbf{b}^\perp), \quad \det(\mathbf{a}, \mathbf{b}) = -\det(\mathbf{b}, \mathbf{a}),$$

which are true for any three planar vectors \mathbf{a} , \mathbf{b} and \mathbf{c} . Namely, (7) is obtained from the first equality applied to $\mathbf{a} = (D_u \mathbf{F}^{(1)}(0, v))^\perp$, $\mathbf{b} = (D_v \mathbf{F}^{(1)}(0, v))^\perp$ and $\mathbf{c} = (D_u \mathbf{F}^{(2)}(0, v))^\perp$ using also that $D_v \mathbf{F}^{(1)}(0, v) = D_v \mathbf{F}^{(2)}(0, v)$, which is true by assumption (3). \square

Lemma 2. *Suppose that $\mathbf{F}^{(\ell)}$ is a bijective and regular C^1 geometry mapping, $\varphi^{(\ell)}$ is a C^1 continuous function and $f^{(\ell)} = \varphi^{(\ell)} \circ \mathbf{F}^{(\ell)}$. Further, let \mathbf{n} be any chosen unit vector. The directional derivative $D_{\mathbf{n}} \varphi^{(\ell)}(x, y)$ at a point $(x, y) = \mathbf{F}^{(\ell)}(u, v)$ is in local coordinates equal to*

$$\omega_{\mathbf{n}}^{(\ell)}(u, v) := \left\langle \mathbf{n}, \mathbf{G}^{(\ell)}(u, v) \right\rangle, \quad (8)$$

where

$$\mathbf{G}^{(\ell)}(u, v) := \frac{1}{\det \mathbf{J} \mathbf{F}^{(\ell)}(u, v)} \left(D_u f^{(\ell)}(u, v) \left(D_v \mathbf{F}^{(\ell)}(u, v) \right)^\perp - D_v f^{(\ell)}(u, v) \left(D_u \mathbf{F}^{(\ell)}(u, v) \right)^\perp \right). \quad (9)$$

Proof. By differentiating the function $f^{(\ell)} = \varphi^{(\ell)} \circ \mathbf{F}^{(\ell)}$ we obtain

$$\left(D_u f^{(\ell)}(u, v), D_v f^{(\ell)}(u, v) \right) = \left(D_x \varphi^{(\ell)} \left(\mathbf{F}^{(\ell)}(u, v) \right), D_y \varphi^{(\ell)} \left(\mathbf{F}^{(\ell)}(u, v) \right) \right) \mathbf{J} \mathbf{F}^{(\ell)}(u, v).$$

Multiplying this equality by the inverse of the Jacobian matrix $\mathbf{J} \mathbf{F}^{(\ell)}(u, v)$ we get that

$$\mathbf{G}^{(\ell)}(u, v) = \left(D_x \varphi^{(\ell)} \left(\mathbf{F}^{(\ell)}(u, v) \right), D_y \varphi^{(\ell)} \left(\mathbf{F}^{(\ell)}(u, v) \right) \right).$$

Applying the scalar product $\langle \mathbf{n}, \cdot \rangle$ on this equation gives

$$\omega_{\mathbf{n}}^{(\ell)}(u, v) = \left\langle \mathbf{n}, \left(D_x \varphi^{(\ell)} \left(\mathbf{F}^{(\ell)}(u, v) \right), D_y \varphi^{(\ell)} \left(\mathbf{F}^{(\ell)}(u, v) \right) \right) \right\rangle = D_{\mathbf{n}} \varphi^{(\ell)}(x, y),$$

where $(x, y) = \mathbf{F}^{(\ell)}(u, v)$ which concludes the proof. \square

Let us now choose a unit vector \mathbf{n} orthogonal to the common edge \mathcal{E} . Multiplying (7) by $\langle \mathbf{n}, \cdot \rangle$ we get that

$$\alpha_3(v) = \alpha_2(v)\beta_1(v) - \alpha_1(v)\beta_2(v), \quad (10)$$

where

$$\beta_\ell(v) = \frac{1}{\beta(v)} \left\langle \mathbf{n}, \left(D_u \mathbf{F}^{(\ell)}(0, v) \right)^\perp \right\rangle, \quad \beta(v) := \left\langle \mathbf{n}, \left(D_v \mathbf{F}^{(1)}(0, v) \right)^\perp \right\rangle = \left\langle \mathbf{n}, \left(D_v \mathbf{F}^{(2)}(0, v) \right)^\perp \right\rangle. \quad (11)$$

The assumption that parameterizations $\mathbf{F}^{(1)}$ and $\mathbf{F}^{(2)}$ are in \mathbb{P}_1^2 or in $\mathbb{P}_{1,1}^2$ implies that $\beta \in \mathbb{P}_0$ is a nonzero constant, the degree of $\alpha_1, \alpha_2, \beta_1, \beta_2$ is less or equal to 1, and the degree of α_3 is less or equal to 2. By (10) the condition (6) rewrites to

$$\alpha_1(v) \left(D_u f^{(2)}(0, v) - \beta_2(v) D_v f^{(1)}(0, v) \right) = \alpha_2(v) \left(D_u f^{(1)}(0, v) - \beta_1(v) D_v f^{(1)}(0, v) \right). \quad (12)$$

On the other hand, using Lemma 2 for $u = 0$, the definitions in (11) and the identity $\det \mathbf{J} \mathbf{F}^{(\ell)}(u, v) = \alpha_\ell(v)$, one can see that the directional derivative $D_{\mathbf{n}} \varphi^{(\ell)}$ at points on the boundary is in local coordinates equal to

$$\omega_{\mathbf{n}}^{(\ell)}(0, v) = \frac{\beta}{\alpha_\ell(v)} \left(D_u f^{(\ell)}(0, v) - \beta_\ell(v) D_v f^{(\ell)}(0, v) \right), \quad \ell = 1, 2. \quad (13)$$

So, from (12) and (13) it follows that the G^1 continuity condition (12) is simply equal to

$$\omega_{\mathbf{n}}^{(1)}(0, v) = \omega_{\mathbf{n}}^{(2)}(0, v), \quad v \in [0, 1],$$

cf. [45]. The additional assumption $D_{\mathbf{n}} \varphi^{(\ell)}|_{\mathcal{E}} \in \mathbb{P}_{p-1}$ implies that

$$\omega_{\mathbf{n}}^{(1)}(0, v) = \omega_{\mathbf{n}}^{(2)}(0, v) = \beta \sum_{j=0}^{p-1} d_j B_j^{p-1}(v), \quad v \in [0, 1], \quad (14)$$

for some coefficients d_j , $j = 0, 1, \dots, p-1$.

In the following subsections we analyze the continuity conditions across the common edge in more detail for three different types of element pairs: quadrilateral–triangle, triangle–triangle and quadrilateral–quadrilateral. According to the simplified notation introduced in this section, we denote the common edge of $\Omega^{(1)}$ and $\Omega^{(2)}$ by $\mathcal{E} = \mathcal{E}(\mathbf{V}^{(1)}, \mathbf{V}^{(2)})$, and we choose \mathbf{n} as the vector orthogonal to \mathcal{E} , i.e.,

$$\mathbf{n} = \left(\mathbf{V}^{(2)} - \mathbf{V}^{(1)} \right)^\perp / \|\mathbf{V}^{(2)} - \mathbf{V}^{(1)}\|.$$

3.2. Quadrilateral–triangle

Suppose that $\Omega^{(1)}$ is a quadrilateral and $\Omega^{(2)}$ a triangle,

$$\Omega^{(1)} = \mathcal{Q}(\mathbf{V}^{(1)}, \mathbf{V}^{(2)}, \mathbf{V}^{(3)}, \mathbf{V}^{(4)}), \quad \Omega^{(2)} = \mathcal{T}(\mathbf{V}^{(5)}, \mathbf{V}^{(2)}, \mathbf{V}^{(1)}), \quad (15)$$

and let the geometry mappings be equal to

$$\begin{aligned} \mathbf{F}^{(1)}(u, v) &= (1-u)(1-v)\mathbf{V}^{(1)} + (1-u)v\mathbf{V}^{(2)} + uv\mathbf{V}^{(3)} + u(1-v)\mathbf{V}^{(4)}, \\ \mathbf{F}^{(2)}(u, v) &= u\mathbf{V}^{(5)} + v\mathbf{V}^{(2)} + (1-u-v)\mathbf{V}^{(1)}. \end{aligned} \quad (16)$$

This configuration is visualized in Figure 4.

Remark 1. Note that the parameters of the geometry mapping $\mathbf{F}^{(2)}$ define the triple $(u, v, 1-u-v)$ which represent the barycentric coordinates of the point $\mathbf{F}^{(2)}(u, v)$ with respect to the triangle $\mathcal{T}(\mathbf{V}^{(5)}, \mathbf{V}^{(2)}, \mathbf{V}^{(1)})$.

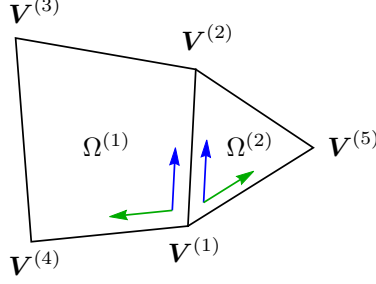


Figure 4: A quadrilateral-triangle pair with parameter directions for u (green) and v (blue).

The gluing functions α_1, α_3 are in this case linear polynomials $\alpha_i(v) = (1-v)\alpha_{i,0} + v\alpha_{i,1}$, $i = 1, 3$, with coefficients

$$\begin{aligned}\alpha_{1,0} &= \det \left[\mathbf{V}^{(4)} - \mathbf{V}^{(1)}, \mathbf{V}^{(2)} - \mathbf{V}^{(1)} \right], & \alpha_{1,1} &= \det \left[\mathbf{V}^{(3)} - \mathbf{V}^{(2)}, \mathbf{V}^{(2)} - \mathbf{V}^{(1)} \right], \\ \alpha_{3,0} &= \det \left[\mathbf{V}^{(5)} - \mathbf{V}^{(1)}, \mathbf{V}^{(4)} - \mathbf{V}^{(1)} \right], & \alpha_{3,1} &= \det \left[\mathbf{V}^{(5)} - \mathbf{V}^{(1)}, \mathbf{V}^{(3)} - \mathbf{V}^{(2)} \right],\end{aligned}$$

while α_2 reduces to a nonzero constant, $\alpha_2 = \det \left[\mathbf{V}^{(5)} - \mathbf{V}^{(1)}, \mathbf{V}^{(2)} - \mathbf{V}^{(1)} \right]$. Moreover, from (13) we see that $\beta, \beta_2 \in \mathbb{P}_0$, $\beta_1 \in \mathbb{P}_1$,

$$\begin{aligned}\beta &= \|\mathbf{V}^{(2)} - \mathbf{V}^{(1)}\|, & \beta_2 &= \frac{\langle \mathbf{V}^{(2)} - \mathbf{V}^{(1)}, \mathbf{V}^{(5)} - \mathbf{V}^{(1)} \rangle}{\|\mathbf{V}^{(2)} - \mathbf{V}^{(1)}\|^2}, \\ \beta_1(v) &= (1-v)\beta_{1,0} + v\beta_{1,1}, & \beta_{1,0} &= \frac{\langle \mathbf{V}^{(2)} - \mathbf{V}^{(1)}, \mathbf{V}^{(4)} - \mathbf{V}^{(1)} \rangle}{\|\mathbf{V}^{(2)} - \mathbf{V}^{(1)}\|^2}, & \beta_{1,1} &= \frac{\langle \mathbf{V}^{(2)} - \mathbf{V}^{(1)}, \mathbf{V}^{(3)} - \mathbf{V}^{(2)} \rangle}{\|\mathbf{V}^{(2)} - \mathbf{V}^{(1)}\|^2}.\end{aligned}$$

Let $f^{(1)}$ be a bivariate polynomial of bi-degree (p, p) and let $f^{(2)}$ be a bivariate polynomial of total degree p , expressed in a Bernstein basis as

$$f^{(1)}(u, v) = \sum_{i,j=0}^p b_{i,j}^{(1)} B_i^p(u) B_j^p(v), \quad f^{(2)}(u, v) = \sum_{i+j+k=p} b_{i,j,k}^{(2)} B_{i,j,k}^{\triangle,p}(u, v). \quad (17)$$

It is straightforward to compute

$$\begin{aligned}f^{(1)}(0, v) &= \sum_{j=0}^p b_{0,j}^{(1)} B_j^p(v), & f^{(2)}(0, v) &= \sum_{j=0}^p b_{0,j,p-j}^{(2)} B_j^p(v), \\ D_u f^{(1)}(0, v) &= p \sum_{j=0}^p \left(b_{1,j}^{(1)} - b_{0,j}^{(1)} \right) B_j^p(v), & D_v f^{(1)}(0, v) &= p \sum_{j=0}^{p-1} \left(b_{0,j+1}^{(1)} - b_{0,j}^{(1)} \right) B_j^{p-1}(v), \\ D_u f^{(2)}(0, v) &= p \sum_{j=0}^{p-1} \left(b_{1,j,p-1-j}^{(2)} - b_{0,j,p-j}^{(2)} \right) B_j^{p-1}(v), & D_v f^{(2)}(0, v) &= p \sum_{j=0}^{p-1} \left(b_{0,j+1,p-1-j}^{(2)} - b_{0,j,p-j}^{(2)} \right) B_j^{p-1}(v).\end{aligned}$$

Thus the condition (5) is fulfilled iff

$$b_{0,j}^{(1)} = b_{0,j,p-j}^{(2)} = c_j, \quad j = 0, 1, \dots, p, \quad (18)$$

for any chosen values c_j . Since in this case α_2 and β_2 are constants, we can see that $w_{\mathbf{n}}^{(2)}(0, \cdot) \in \mathbb{P}_{p-1}$, so the condition $D_{\mathbf{n}\varphi^{(i)}}|_{\mathcal{E}} \in \mathbb{P}_{p-1}$ is automatically fulfilled. Relations (13) and (14) imply

$$D_u f^{(1)}(0, v) - \beta_1(v) D_v f^{(1)}(0, v) = \alpha_1(v) \sum_{j=0}^{p-1} d_j B_j^{p-1}(v) \quad (19a)$$

and

$$D_u f^{(2)}(0, v) - \beta_2 D_v f^{(2)}(0, v) = \alpha_2 \sum_{j=0}^{p-1} d_j B_j^{p-1}(v), \quad (19b)$$

which together with (18), (19) and

$$\begin{aligned} \alpha_1(v) \sum_{j=0}^{p-1} d_j B_j^{p-1}(v) &= \sum_{j=0}^p \frac{1}{p} ((p-j) \alpha_{1,0} d_j + j \alpha_{1,1} d_{j-1}) B_j^p(v), \\ \beta_1(v) D_v f^{(1)}(0, v) &= \sum_{j=0}^p \left((p-j) \beta_{1,0} (b_{0,j+1}^{(1)} - b_{0,j}^{(1)}) + j \beta_{1,1} (b_{0,j}^{(1)} - b_{0,j-1}^{(1)}) \right) B_j^p(v), \end{aligned}$$

determines the Bézier ordinates

$$b_{1,j}^{(1)} = c_j + \frac{1}{p} \left(\frac{1}{p} ((p-j) \alpha_{1,0} d_j + j \alpha_{1,1} d_{j-1}) + (p-j) \beta_{1,0} (c_{j+1} - c_j) + j \beta_{1,1} (c_j - c_{j-1}) \right) \quad (20)$$

for $j = 0, 1, \dots, p$, and

$$b_{1,j,p-1-j}^{(2)} = c_j + \beta_2 (c_{j+1} - c_j) + \frac{1}{p} \alpha_2 d_j, \quad j = 0, 1, \dots, p-1, \quad (21)$$

where $c_{-1} := 0$, $c_{p+1} := 0$. We can summarize the obtained results in the following proposition.

Proposition 1. *Assume that the two neighboring patches, corresponding geometry mappings and functions $f^{(1)}$, $f^{(2)}$ are given by (15), (16) and (17). Then the isoparametric function (4) is C^1 continuous across the common interface iff the control ordinates satisfy (18), (20) and (21) for any chosen $2p+1$ coefficients $(c_i)_{i=0}^p$ and $(d_i)_{i=0}^{p-1}$.*

3.3. Triangle-triangle

Suppose that $\Omega^{(1)}$ and $\Omega^{(2)}$ are both triangles,

$$\Omega^{(1)} = \mathcal{T}(\mathbf{V}^{(3)}, \mathbf{V}^{(2)}, \mathbf{V}^{(1)}), \quad \Omega^{(2)} = \mathcal{T}(\mathbf{V}^{(5)}, \mathbf{V}^{(2)}, \mathbf{V}^{(1)}), \quad (22)$$

and the geometry mappings equal

$$\mathbf{F}^{(1)}(u, v) = u \mathbf{V}^{(3)} + v \mathbf{V}^{(2)} + (1-u-v) \mathbf{V}^{(1)}, \quad \mathbf{F}^{(2)}(u, v) = u \mathbf{V}^{(5)} + v \mathbf{V}^{(2)} + (1-u-v) \mathbf{V}^{(1)}. \quad (23)$$

This configuration is visualized in Figure 5.

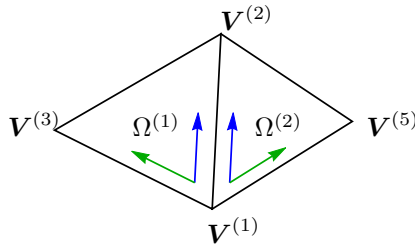


Figure 5: A triangle-triangle pair with parameter directions for u (green) and v (blue).

The gluing functions α_i , $i = 1, 2, 3$, as well as β_1 , β_2 are in this case constants,

$$\begin{aligned} \alpha_1 &= \det [\mathbf{V}^{(3)} - \mathbf{V}^{(1)}, \mathbf{V}^{(2)} - \mathbf{V}^{(1)}], \quad \alpha_2 = \det [\mathbf{V}^{(5)} - \mathbf{V}^{(1)}, \mathbf{V}^{(2)} - \mathbf{V}^{(1)}], \\ \alpha_3 &= \det [\mathbf{V}^{(5)} - \mathbf{V}^{(1)}, \mathbf{V}^{(3)} - \mathbf{V}^{(1)}], \\ \beta_1 &= \frac{1}{\|\mathbf{V}^{(2)} - \mathbf{V}^{(1)}\|} \langle \mathbf{V}^{(2)} - \mathbf{V}^{(1)}, \mathbf{V}^{(3)} - \mathbf{V}^{(1)} \rangle, \quad \beta_2 = \frac{1}{\|\mathbf{V}^{(2)} - \mathbf{V}^{(1)}\|} \langle \mathbf{V}^{(2)} - \mathbf{V}^{(1)}, \mathbf{V}^{(5)} - \mathbf{V}^{(1)} \rangle. \end{aligned}$$

Further, let

$$f^{(\ell)}(u, v) = \sum_{i+j+k=p} b_{i,j,k}^{(\ell)} B_{i,j,k}^{\triangle,p}(u, v), \quad \ell = 1, 2. \quad (24)$$

Also in this case the condition $D_{\mathbf{n}} \varphi^{(\ell)}|_{\mathcal{E}} \in \mathbb{P}_{p-1}$ is fulfilled automatically and independently of the geometry of a mesh, and it is straightforward to derive the following result.

Proposition 2. *Assume that the two neighboring patches, corresponding geometry mappings and functions $f^{(1)}, f^{(2)}$ are given by (22), (23) and (24). Then the isoparametric function (4) is C^1 continuous across the common interface iff the control ordinates satisfy*

$$b_{0,j,p-j}^{(1)} = b_{0,j,p-j}^{(2)} = c_j, \quad j = 0, 1, \dots, p, \quad (25)$$

$$b_{1,j,p-1-j}^{(\ell)} = c_j + \beta_\ell (c_{j+1} - c_j) + \frac{1}{p} \alpha_\ell d_j, \quad j = 0, 1, \dots, p-1, \quad \ell = 1, 2, \quad (26)$$

for any chosen $2p+1$ coefficients $(c_i)_{i=0}^p$ and $(d_i)_{i=0}^{p-1}$.

Proof. Since $f^{(\ell)}(0, v) = \sum_{j=0}^p b_{0,j,p-j}^{(\ell)} B_j^p(v)$, $\ell = 1, 2$, we get (25). Additionally, for $\ell = 1, 2$, we have

$$D_u f^{(\ell)}(0, v) = p \sum_{j=0}^{p-1} \left(b_{1,j,p-1-j}^{(\ell)} - b_{0,j,p-j}^{(\ell)} \right) B_j^{p-1}(v), \quad D_v f^{(\ell)}(0, v) = p \sum_{j=0}^{p-1} \left(b_{0,j+1,p-1-j}^{(\ell)} - b_{0,j,p-j}^{(\ell)} \right) B_j^{p-1}(v), \quad (27)$$

and (13)–(14) imply

$$D_u f^{(\ell)}(0, v) - \beta_\ell D_v f^{(\ell)}(0, v) = \alpha_\ell \sum_{j=0}^{p-1} d_j B_j^{p-1}(v), \quad \ell = 1, 2, \quad (28)$$

for constants $\alpha_1, \alpha_2, \beta_1, \beta_2$. Inserting (27) into (28) finally proves (26). \square

3.4. Quadrilateral–quadrilateral

Suppose that $\Omega^{(1)}$ and $\Omega^{(2)}$ are both quadrilaterals,

$$\Omega^{(1)} = \mathcal{Q}(\mathbf{V}^{(1)}, \mathbf{V}^{(2)}, \mathbf{V}^{(3)}, \mathbf{V}^{(4)}), \quad \Omega^{(2)} = \mathcal{Q}(\mathbf{V}^{(1)}, \mathbf{V}^{(2)}, \mathbf{V}^{(5)}, \mathbf{V}^{(6)}), \quad (29)$$

and the geometry mappings equal

$$\begin{aligned} \mathbf{F}^{(1)}(u, v) &= (1-u)(1-v)\mathbf{V}^{(1)} + (1-u)v\mathbf{V}^{(2)} + uv\mathbf{V}^{(3)} + u(1-v)\mathbf{V}^{(4)}, \\ \mathbf{F}^{(2)}(u, v) &= (1-u)(1-v)\mathbf{V}^{(1)} + (1-u)v\mathbf{V}^{(2)} + uv\mathbf{V}^{(5)} + u(1-v)\mathbf{V}^{(6)}. \end{aligned} \quad (30)$$

This configuration is visualized in Figure 6.

Now, the functions α_i, β_i , $i = 1, 2$, are linear polynomials

$$\begin{aligned} \alpha_i(v) &= (1-v)\alpha_{i,0} + v\alpha_{i,1}, \\ \alpha_{i,0} &= \det[\mathbf{V}^{(2+2i)} - \mathbf{V}^{(1)}, \mathbf{V}^{(2)} - \mathbf{V}^{(1)}], \quad \alpha_{i,1} = \det[\mathbf{V}^{(1+2i)} - \mathbf{V}^{(2)}, \mathbf{V}^{(2)} - \mathbf{V}^{(1)}], \\ \beta_i(v) &= (1-v)\beta_{i,0} + v\beta_{i,1}, \\ \beta_{i,0} &= \frac{\langle \mathbf{V}^{(2)} - \mathbf{V}^{(1)}, \mathbf{V}^{(2+2i)} - \mathbf{V}^{(1)} \rangle}{\|\mathbf{V}^{(2)} - \mathbf{V}^{(1)}\|^2}, \quad \beta_{i,1} = \frac{\langle \mathbf{V}^{(2)} - \mathbf{V}^{(1)}, \mathbf{V}^{(1+2i)} - \mathbf{V}^{(2)} \rangle}{\|\mathbf{V}^{(2)} - \mathbf{V}^{(1)}\|^2}, \end{aligned}$$

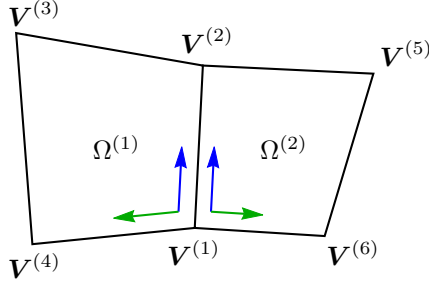


Figure 6: A quadrilateral–quadrilateral pair with parameter directions for u (green) and v (blue).

while $\alpha_3 \in \mathbb{P}_2$. Let $f^{(1)}$ and $f^{(2)}$ be two bivariate polynomials of bi-degree (p, p) ,

$$f^{(\ell)}(u, v) = \sum_{i,j=0}^p b_{i,j}^{(\ell)} B_i^p(u) B_j^p(v), \quad \ell = 1, 2. \quad (31)$$

In this case it could happen that $D_{\mathbf{n}} \varphi^{(\ell)}|_{\mathcal{E}}$ would be of degree p , not $p-1$. In particular, this can happen if α_ℓ reduces to a constant, which, for $\ell = 1$, happens if $\mathcal{E}(\mathbf{V}^{(1)}, \mathbf{V}^{(2)})$ is parallel to $\mathcal{E}(\mathbf{V}^{(3)}, \mathbf{V}^{(4)})$, and for $\ell = 2$ if $\mathcal{E}(\mathbf{V}^{(1)}, \mathbf{V}^{(2)})$ is parallel to $\mathcal{E}(\mathbf{V}^{(5)}, \mathbf{V}^{(6)})$. Moreover, in certain configurations, α_1 and α_2 are linearly dependent, with $\alpha_2(v) = \lambda \alpha_1(v)$ and can thus be replaced by $\alpha'_1 \equiv 1$ and $\alpha'_2 \equiv \lambda$. E.g. if both elements are rectangles, we have constant α_ℓ and $\beta_\ell \equiv 0$. See [4, 29] for a more detailed study of the possible cases. So, the additional condition $D_{\mathbf{n}} \varphi^{(\ell)}|_{\mathcal{E}} \in \mathbb{P}_{p-1}$ is included to make the proceeding construction independent of the geometry of the mesh.

Proposition 3. *Assume that the two neighboring elements, corresponding geometry mappings and functions $f^{(1)}$, $f^{(2)}$ are given by (29), (30) and (31). Then the isoparametric function (4) is C^1 continuous across the common interface and satisfies the additional condition that $D_{\mathbf{n}} \varphi^{(\ell)}|_{\mathcal{E}} \in \mathbb{P}_{p-1}$, iff the control ordinates satisfy*

$$\begin{aligned} b_{0,j}^{(1)} &= b_{0,j}^{(2)} = c_j, \\ b_{1,j}^{(\ell)} &= c_j + \frac{1}{p} \left(\frac{1}{p} ((p-j) \alpha_{\ell,0} d_j + j \alpha_{\ell,1} d_{j-1}) + (p-j) \beta_{\ell,0} (c_{j+1} - c_j) + j \beta_{\ell,1} (c_j - c_{j-1}) \right), \quad \ell = 1, 2, \end{aligned} \quad (32)$$

$j = 0, 1, \dots, p$, for any chosen $2p+1$ coefficients $(c_i)_{i=0}^p$ and $(d_i)_{i=0}^{p-1}$.

Proof. Since $\Omega^{(1)}$ and $\Omega^{(2)}$ are both quadrilaterals, we have $f^{(\ell)}(0, v) = \sum_{j=0}^p b_{0,j}^{(\ell)} B_j^p(v)$,

$$D_u f^{(\ell)}(0, v) = p \sum_{j=0}^p (b_{1,j}^{(\ell)} - b_{0,j}^{(\ell)}) B_j^p(v), \quad D_v f^{(\ell)}(0, v) = p \sum_{j=0}^{p-1} (b_{0,j+1}^{(\ell)} - b_{0,j}^{(\ell)}) B_j^{p-1}(v),$$

for $\ell = 1, 2$. Assuming $D_{\mathbf{n}} \varphi^{(\ell)}|_{\mathcal{E}} \in \mathbb{P}_{p-1}$, it must hold that

$$D_u f^{(\ell)}(0, v) - \beta_\ell(v) D_v f^{(\ell)}(0, v) = \alpha_\ell(v) \sum_{j=0}^{p-1} d_j B_j^{p-1}(v), \quad \ell = 1, 2,$$

for linear α_ℓ , β_ℓ , $\ell = 1, 2$, which is further equivalent to (32). \square

In Figure 7 we plot pairs of elements, triangle–quadrilateral (left), triangle–triangle (center) as well as quadrilateral–quadrilateral (right). For some coefficients c_i and d_i we plot the relevant, non-vanishing Bézier ordinates in blue and green, respectively. The figure is to be interpreted in the following way: if all

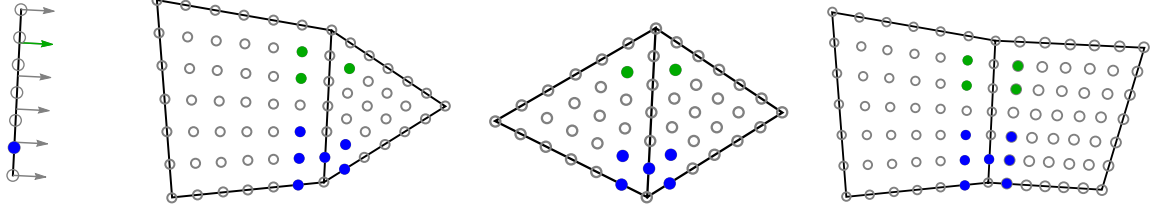


Figure 7: Pairs of elements with non-vanishing Bézier ordinates for given coefficients c_1 (in blue) and d_4 (in green). Note that the structure of non-vanishing ordinates is always the same, only shifted by the given index. In the given configurations we have $p = 6$. The underlying control structure is plotted on the left: the coefficients c_i (controlling function values along the interface) are depicted as circles and the coefficients d_j (controlling crossing derivatives) as arrows. Each coefficient (control variable) c_i or d_j generates one function over the respective element pair.

coefficients c_i and d_i are set to zero, except for c_1 , then only the Bézier ordinates depicted in blue are non-vanishing. On the other hand, if all coefficients except for d_4 are set to zero, then only the green ordinates are non-vanishing. As one can see in Figure 7, the C^1 functions across an interface couple degrees of freedom in a non-trivial way. The dimension of the C^1 space around a given vertex and the construction of a basis depends on the geometry, i.e. on the exact configuration of elements around the vertex. In order to simplify the construction, we demand C^2 continuity at vertices, thus fixing the dimension of the space and avoiding special cases. This strategy of imposing super-smoothness is a common tool for triangle meshes, see [12, 38] or [32] for spline patches. This leads us to the interpolation problem as described in the following section.

4. Analysis of the Argyris-like space

In order to analyze the properties of the space \mathcal{A}_p (defined in (2)), we formulate an interpolation problem that uniquely characterizes the elements of the spline space. The interpolation problem provides the dimension formula for \mathcal{A}_p and gives rise to a projection operator that is used to prove the approximation properties of the space.

4.1. Interpolation problem

The following theorem states how the elements of \mathcal{A}_p can be described in terms of interpolation data provided at the vertices, along the edges and in the interior of the mixed mesh.

Recall that a point set is called *unisolvent* in a function space, if any function in the space is uniquely determined by interpolating the values at the points in this set.

Theorem 1. *Let $\Omega \subset \mathbb{R}^2$ be an open domain on which a mixed mesh, satisfying (1), is defined. Then there exists a unique isoparametric spline function $\varphi \in \mathcal{A}_p$, $p \geq 5$, that satisfies the following interpolation conditions:*

(A) *For every vertex $\mathbf{V}^{(i)}$, $i \in \mathcal{I}_V$, let*

$$D_x^a D_y^b \varphi \left(\mathbf{V}^{(i)} \right) = \sigma_{i,a,b}, \quad 0 \leq a + b \leq 2,$$

for some given values $\sigma_{i,a,b} \in \mathbb{R}$.

(B) *For every edge $\mathcal{E}^{(i)}$, $i \in \mathcal{I}_E$, choose $p - 5$ pairwise different points $\mathbf{R}_\ell^{(i)} \in \mathcal{E}^{(i)}$, $\ell = 1, 2, \dots, p - 5$, as well as $p - 4$ pairwise different points $\mathbf{S}_\ell^{(i)} \in \mathcal{E}^{(i)}$, $\ell = 1, 2, \dots, p - 4$, and let*

$$\varphi \left(\mathbf{R}_\ell^{(i)} \right) = \sigma_{i,\ell}, \quad \ell = 1, 2, \dots, p - 5, \quad D_{\mathbf{n}_i} \varphi \left(\mathbf{S}_\ell^{(i)} \right) = w_{i,\ell}, \quad \ell = 1, 2, \dots, p - 4,$$

for some given values $\sigma_{i,\ell}, w_{i,\ell} \in \mathbb{R}$.

(C) For every quadrilateral element $\Omega^{(i)}$, $i \in \mathcal{I}_\square$, choose $(p-3)^2$ pairwise different points

$$\mathbf{Q}_{\ell,k}^{(i)} = \mathbf{F}^{(i)} \left(\widehat{\mathbf{Q}}_{\ell,k}^{(i)} \right), \quad \ell, k = 1, 2, \dots, p-3,$$

where $\widehat{\mathbf{Q}}_{\ell,k}^{(i)}$ are unisolvent in $\text{span}_{2 \leq j_1, j_2 \leq p-2} (B_{j_1, j_2}^{p,p})$, and let

$$\varphi \left(\mathbf{Q}_{\ell,k}^{(i)} \right) = \sigma_{i,\ell,k}^\square, \quad \ell, k = 1, 2, \dots, p-3,$$

for some given values $\sigma_{i,\ell,k}^\square \in \mathbb{R}$.

(D) For every triangular element $\Omega^{(i)}$, with $i \in \mathcal{I}_\triangle$, choose $\binom{p-4}{2}$ pairwise different points

$$\mathbf{Q}_{\ell,k}^{(i)} = \mathbf{F}^{(i)} \left(\widehat{\mathbf{Q}}_{\ell,k}^{(i)} \right), \quad \ell = 1, 2, \dots, p-5, \quad k = 1, 2, \dots, p-4-\ell,$$

where $\widehat{\mathbf{Q}}_{\ell,k}^{(i)}$ are unisolvent in $\text{span}_{\substack{2 \leq j_1, j_2, j_3 \\ j_1 + j_2 + j_3 = p}} (B_{j_1, j_2, j_3}^{\triangle, p})$, and let

$$\varphi \left(\mathbf{Q}_{\ell,k}^{(i)} \right) = \sigma_{i,\ell,k}^\triangle, \quad \ell = 1, 2, \dots, p-5, \quad k = 1, 2, \dots, p-4-\ell,$$

for some given values $\sigma_{i,\ell,k}^\triangle \in \mathbb{R}$.

Proof. We need to show that the interpolation conditions (A)–(D) uniquely determine the bivariate polynomial on every patch $\overline{\Omega^{(i)}} = \mathbf{F}^{(i)}(\mathcal{D}^{(i)})$, $i \in \mathcal{I}_\square \cup \mathcal{I}_\triangle$, and that the continuity conditions are satisfied. Let $\mathbf{V}^{(j)}$ be a vertex of $\overline{\Omega^{(i)}}$, obtained as $\mathbf{V}^{(j)} = \mathbf{F}^{(i)}(u_j^{(i)}, v_j^{(i)})$ for some

$$\mathbf{u}_j^{(i)} := (u_j^{(i)}, v_j^{(i)}) \in \{(0,0), (0,1), (1,0), (1,1)\}.$$

From conditions in (A) we get

$$\text{grad } \varphi \left(\mathbf{V}^{(j)} \right) = (\sigma_{j,1,0}, \sigma_{j,0,1}), \quad \mathbf{H}\varphi \left(\mathbf{V}^{(j)} \right) = \begin{bmatrix} \sigma_{j,2,0} & \sigma_{j,1,1} \\ \sigma_{j,1,1} & \sigma_{j,0,2} \end{bmatrix},$$

and from

$$\begin{aligned} \text{grad } f^{(i)} \left(\mathbf{u}_j^{(i)} \right) &= \text{grad } \varphi \left(\mathbf{V}^{(j)} \right) \cdot \mathbf{J}\mathbf{F}^{(i)} \left(\mathbf{u}_j^{(i)} \right) =: (s_{j,1,0}^{(i)}, s_{j,0,1}^{(i)}) =: \mathbf{s}_j^{(i)}, \\ \mathbf{H}f^{(i)} \left(\mathbf{u}_j^{(i)} \right) &= \mathbf{J}\mathbf{F}^{(i)} \left(\mathbf{u}_j^{(i)} \right)^T \cdot \mathbf{H}\varphi \left(\mathbf{V}^{(j)} \right) \cdot \mathbf{J}\mathbf{F}^{(i)} \left(\mathbf{u}_j^{(i)} \right) + \\ &+ D_x \varphi \left(\mathbf{V}^{(j)} \right) \mathbf{H}\mathbf{F}_1^{(i)} \left(\mathbf{u}_j^{(i)} \right) + D_y \varphi \left(\mathbf{V}^{(j)} \right) \mathbf{H}\mathbf{F}_2^{(i)} \left(\mathbf{u}_j^{(i)} \right) =: \begin{bmatrix} s_{j,2,0}^{(i)} & s_{j,1,1}^{(i)} \\ s_{j,1,1}^{(i)} & s_{j,0,2}^{(i)} \end{bmatrix} =: \mathbf{S}_j^{(i)}, \end{aligned}$$

we obtain the C^2 interpolation conditions for $f^{(i)}$ at $\mathbf{u}_j^{(i)}$, i.e.,

$$D_u^a D_v^b f^{(i)} \left(\mathbf{u}_j^{(i)} \right) = s_{j,a,b}^{(i)}, \quad 0 \leq a+b \leq 2.$$

Further, let $\mathcal{E}^{(k)}$, $k \in \mathcal{I}_\mathcal{E}$, be any edge of $\overline{\Omega^{(i)}}$, with boundary vertices $\mathbf{V}^{(k_0)}, \mathbf{V}^{(k_1)}$, $k_0, k_1 \in \mathcal{I}_\mathbf{V}$, parameterized as

$$\mathcal{E}^{(k)} = \left\{ \mathbf{F}^{(i)} \left(\boldsymbol{\epsilon}^{(k)}(t) \right) : t \in (0,1) \right\}, \quad \boldsymbol{\epsilon}^{(k)}(t) := (1-t) \mathbf{u}_{k_0}^{(i)} + t \mathbf{u}_{k_1}^{(i)},$$

and let

$$\theta_k(t) := \sum_{\ell=0}^p c_\ell^{(k)} B_\ell^p(t) = f^{(i)}(\epsilon^{(k)}(t)), \quad \omega_k(t) := \sum_{\ell=0}^{p-1} d_\ell^{(k)} B_\ell^{p-1}(t) = D_{\mathbf{n}_k} \varphi \left(\mathbf{F}^{(i)}(\epsilon^{(k)}(t)) \right), \quad t \in [0, 1],$$

be the restriction of φ and $D_{\mathbf{n}_k} \varphi$ on the edge $\mathcal{E}^{(k)}$ expressed in local coordinates. Further, let $t_{k,\ell}^{(i)}$ be the parameters, such that $\mathbf{R}_{k,\ell} = \mathbf{F}^{(i)}(\epsilon^{(k)}(t_{k,\ell}^{(i)}))$. From (A) and (B) we get $p+1$ conditions

$$\begin{aligned} \theta_k(\ell) &= \sigma_{k,\ell,0,0}, \quad \theta'_k(\ell) = \left\langle \mathbf{s}_{k_\ell}^{(i)}, \mathbf{u}_{k_1}^{(i)} - \mathbf{u}_{k_0}^{(i)} \right\rangle, \quad \theta''_k(\ell) = \left\langle \mathbf{u}_{k_1}^{(i)} - \mathbf{u}_{k_0}^{(i)}, S_{k_\ell}^{(i)} \left(\mathbf{u}_{k_1}^{(i)} - \mathbf{u}_{k_0}^{(i)} \right)^T \right\rangle, \quad \ell = 0, 1, \\ \theta_k(t_{k,\ell}^{(i)}) &= \sigma_{k,\ell}, \quad \ell = 1, 2, \dots, p-5, \end{aligned}$$

which uniquely determine θ_k . Note that $\mathbf{u}_{k_1}^{(i)} - \mathbf{u}_{k_0}^{(i)} \in \{(\pm 1, 0), (0, \pm 1), \pm(1, -1)\}$. From (8) it is straightforward to see that (A) and (B) give also the values of $\mathbf{G}^{(k)}$, $D_u \mathbf{G}^{(k)}$ and $D_v \mathbf{G}^{(k)}$ at $\mathbf{u}_{k_0}^{(i)}, \mathbf{u}_{k_1}^{(i)}$, where $\mathbf{G}^{(k)}$ is defined in (9). The conditions

$$\begin{aligned} \omega_k(\ell) &= \left\langle \mathbf{n}_k, \mathbf{G}^{(k)}(\mathbf{u}_{k_\ell}^{(i)}) \right\rangle, \quad \ell = 0, 1, \\ \omega'_k(\ell) &= \left(\mathbf{u}_{k_1}^{(i)} - \mathbf{u}_{k_0}^{(i)} \right) \left\langle \mathbf{n}_k, D_u \mathbf{G}^{(k)}(\mathbf{u}_{k_\ell}^{(i)}) \right\rangle + \left(\mathbf{v}_{k_1}^{(i)} - \mathbf{v}_{k_0}^{(i)} \right) \left\langle \mathbf{n}_k, D_v \mathbf{G}^{(k)}(\mathbf{u}_{k_\ell}^{(i)}) \right\rangle, \quad \ell = 0, 1, \\ \omega_k(t_{k,\ell}^{(i)}) &= w_{k,\ell}, \quad \ell = 1, 2, \dots, p-4, \end{aligned}$$

then uniquely determine w_k .

Suppose now that $i \in \mathcal{I}_\square$ and $f^{(i)}(u, v) = \sum_{j,\ell=0}^p b_{j,\ell}^{(i)} B_j^p(u) B_\ell^p(v)$. Following Proposition 1, 2 and 3 we see that polynomials θ_k and w_k uniquely determine the ordinates $b_{j,\ell}^{(i)}$ and $b_{\ell,j}^{(i)}$ for $\ell = 0, 1, p-1, p$, $j = 0, 1, \dots, p$. The remaining $(p-3)^2$ ordinates $b_{j,\ell}^{(i)}$, $j, \ell = 2, 3, \dots, p-2$, are computed uniquely from conditions (C). Similarly for $i \in \mathcal{I}_\triangle$ and $f^{(i)}(u, v) = \sum_{j+\ell+r=p} b_{j,\ell,r}^{(i)} B_{j,\ell,r}^{\triangle,p}(u, v)$. Polynomials θ_k and ω_k uniquely determine the ordinates $b_{j,\ell,r}^{(i)}$ with $j, \ell, r \in \{p, p-1\}$, while the remaining ones follow from conditions (D). Since the continuity conditions are satisfied by the construction, the proof is completed. \square

One possible choice for the interpolation points, which we further use in the examples, is the following. For a given edge $\mathcal{E}^{(i)} = \mathcal{E}(\mathbf{V}^{(1)}, \mathbf{V}^{(2)})$ we first compute an equidistant set of points

$$\tilde{\mathbf{R}}_\ell = \frac{2 \lfloor \frac{p}{2} \rfloor - 2 - \ell}{2 \lfloor \frac{p}{2} \rfloor - 2} \left(\frac{p-2}{p} \mathbf{V}^{(1)} + \frac{2}{p} \mathbf{V}^{(2)} \right) + \frac{\ell}{2 \lfloor \frac{p}{2} \rfloor - 2} \left(\frac{2}{p} \mathbf{V}^{(1)} + \frac{p-2}{p} \mathbf{V}^{(2)} \right), \quad \ell = 1, 2, \dots, 2 \lfloor \frac{p}{2} \rfloor - 3.$$

Then for odd degree p we choose

$$\mathbf{R}_\ell^{(i)} := \tilde{\mathbf{R}}_\ell, \quad \ell = 1, \dots, \frac{p-5}{2}, \quad \mathbf{R}_\ell^{(i)} := \tilde{\mathbf{R}}_{\ell+1}, \quad \ell = \frac{p-3}{2}, \dots, p-5, \quad \mathbf{S}_\ell^{(i)} := \tilde{\mathbf{R}}_\ell, \quad \ell = 1, \dots, p-4, \quad (33)$$

and for even p

$$\begin{aligned} \mathbf{R}_\ell^{(i)} &:= \tilde{\mathbf{R}}_\ell, \quad \ell = 1, \dots, \frac{p-6}{2}, \quad \mathbf{R}_{\frac{p-4}{2}}^{(i)} := \tilde{\mathbf{R}}_{\frac{p-2}{2}}, \quad \mathbf{R}_\ell^{(i)} := \tilde{\mathbf{R}}_{\ell+2}, \quad \ell = \frac{p-2}{2}, \dots, p-5, \\ \mathbf{S}_\ell^{(i)} &:= \tilde{\mathbf{R}}_\ell, \quad \ell = 1, \dots, \frac{p-4}{2}, \quad \mathbf{S}_\ell^{(i)} := \tilde{\mathbf{R}}_{\ell+1}, \quad \ell = \frac{p-2}{2}, \dots, p-4. \end{aligned} \quad (34)$$

Additional interpolation points in the interior are chosen as

$$\mathbf{Q}_{\ell,k}^{(i)} := \mathbf{F}^{(i)} \left(\frac{\ell}{p}, \frac{k}{p} \right) \in \Omega^{(i)}, \quad \ell, k = 2, \dots, p-2, \quad (35)$$

for quadrilaterals and

$$\mathbf{Q}_{\ell,k}^{(i)} := \mathbf{F}^{(i)} \left(\frac{\ell}{p}, \frac{k}{p} \right) \in \Omega^{(i)}, \quad \ell = 2, \dots, p-2, \quad k = 2, \dots, p-2-\ell, \quad (36)$$

for triangles. For the graphical interpretation of these interpolation points in the case $p = 8$ and $p = 9$ see Fig. 13.

4.2. Properties of the space \mathcal{A}_p

Due to the interpolation conditions **(A)**–**(D)**, we have the following dimension formula (cf. Fig. 13).

Corollary 1. *The dimension of the space \mathcal{A}_p equals*

$$\dim \mathcal{A}_p = 6 |\mathcal{I}_V| + (2p-9) |\mathcal{I}_E| + (p-3)^2 |\mathcal{I}_\square| + \binom{p-4}{2} |\mathcal{I}_\triangle|.$$

Moreover, the space \mathcal{A}_p contains bivariate polynomials of total degree p .

Lemma 3. *We have $\mathbb{P}_p^2 \subset \mathcal{A}_p$.*

This lemma follows directly from the definition of the space, hence the local space for triangles is equal to \mathbb{P}_p^2 , whereas it contains \mathbb{P}_p^2 for quadrilaterals (see [33]). Another useful consequence of Theorem 1 is the following: based on this theorem we define the global projection operator

$$\Pi_p : C^2(\overline{\Omega}) \rightarrow \mathcal{A}_p \quad (37)$$

that assigns to every function $f \in C^2(\overline{\Omega})$ the C^1 -spline $\Pi_p f \in \mathcal{A}_p$ that satisfies the interpolation conditions **(A)**–**(D)** for data sampled from the function f . We can moreover define the local projection operators

$$\Pi_p^{(i)} : C^2(\overline{\Omega^{(i)}}) \rightarrow \mathcal{A}_p|_{\overline{\Omega^{(i)}}}. \quad (38)$$

By definition we have

$$(\Pi_p \varphi)|_{\overline{\Omega^{(i)}}} = \Pi_p^{(i)}(\varphi|_{\overline{\Omega^{(i)}}}).$$

The global and local projection operators Π_p and $\Pi_p^{(i)}$, respectively, are defined by interpolation using the conditions specified in Theorem 1. In case of the global projector Π_p all interpolation conditions are needed. In case of the local projector $\Pi_p^{(i)}$ only those interpolation conditions are needed, which are defined on $\overline{\Omega^{(i)}}$.

The operator Π_p is bounded, if all elements $\Omega^{(i)}$ of the mesh are shape regular.

Definition 1. *A mesh (or more precisely a sequence of refined meshes) is said to be shape regular, with shape regularity parameter $\rho > 0$, if for each triangle of the mesh all angles are bounded from below by ρ and for each quadrilateral of the mesh all angles of all triangles obtained by splitting the quadrilateral along the two diagonals are bounded from below by ρ , see Figure 8.*

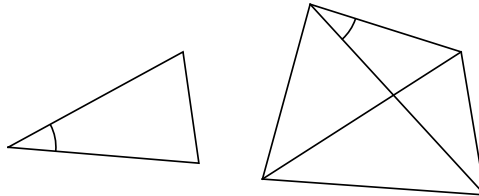


Figure 8: A visualization of the shape regularity condition: the mesh is shape regular if the minimum of all angles as depicted in the two examples is uniformly bounded from below by ρ . The smallest angles for the triangle and quadrilateral are marked.

Given a shape regular mesh, there exists a constant $C(\rho)$, depending only on ρ , such that

$$1 \leq \frac{\max |\det \mathbf{J}\mathbf{F}^{(i)}|}{\min |\det \mathbf{J}\mathbf{F}^{(i)}|} \leq C(\rho)$$

as well as

$$1 \leq \frac{\max_{1 \leq i < j \leq \nu} |\mathbf{V}^{(i)} - \mathbf{V}^{(j)}|}{\min_{1 \leq i < j \leq \nu} |\mathbf{V}^{(i)} - \mathbf{V}^{(j)}|} \leq C(\rho),$$

where $\nu = 3$ and $\Omega^{(i)} = \mathcal{T}(\mathbf{V}^{(1)}, \mathbf{V}^{(2)}, \mathbf{V}^{(3)})$ for triangles and $\nu = 4$ and $\Omega^{(i)} = \mathcal{Q}(\mathbf{V}^{(1)}, \mathbf{V}^{(2)}, \mathbf{V}^{(3)}, \mathbf{V}^{(4)})$ for quadrilaterals. In the following we denote by $|\cdot|_{H^\ell(D)}$ the H^ℓ -seminorm, where $|\cdot|_{H^\ell(D)}^2$ is the sum of squares of L^2 -norms of all derivatives of order ℓ over the domain D , and by

$$\|\varphi\|_{H^m(D)} = \left(\sum_{\ell=0}^m |\varphi|_{H^\ell(D)}^2 \right)^{\frac{1}{2}}$$

the H^m -norm. We have the following lemma for shape regular elements.

Lemma 4. *Let $\Omega^{(i)}$ be any mesh element and let $\mathbf{R}_\ell^{(i)}$, $\mathbf{S}_\ell^{(i)}$ and $\mathbf{Q}_{\ell,k}^{(i)}$ be defined by (33)–(36). Then the local projector as defined in (38) satisfies*

$$\|\Pi_p^{(i)} \psi\|_{H^2(\Omega^{(i)})} \leq \sigma \|\psi\|_{C^2(\overline{\Omega^{(i)}})},$$

as well as

$$\|\Pi_p^{(i)} \psi\|_{L^\infty(\Omega^{(i)})} \leq \sigma \|\psi\|_{C^2(\overline{\Omega^{(i)}})},$$

where σ depends only on the degree p , on the element size $\text{diam}(\Omega^{(i)})$ and on the shape regularity constant ρ and where $\|\psi\|_{C^2(\overline{\Omega^{(i)}})}$ takes the supremum of all derivatives up to second order on the element $\Omega^{(i)}$.

Proof. A proof of this lemma can be found in [33] for quadrilaterals. Here, for the sake of completeness, we repeat and extend it shortly to triangles. Assume that the degree p is fixed. For each element $\Omega^{(i)}$ there exists a constant $C(\Omega^{(i)}) \in \mathbb{R}$, such that

$$\max \left(\|\Pi_p^{(i)} \psi\|_{H^2(\Omega^{(i)})}, \|\Pi_p^{(i)} \psi\|_{L^\infty(\Omega^{(i)})} \right) \leq C(\Omega^{(i)}) \|\psi\|_{C^2(\overline{\Omega^{(i)}})}.$$

This follows directly from Theorem 1 as the projector $\Pi_p^{(i)}$ is well-defined, yields a bounded (mapped) polynomial and is completely determined by values, first and second derivatives of ψ in $\Omega^{(i)}$. Note that the definition of the projector is invariant with respect to translations of the element $\Omega^{(i)}$. Thus, the element may be moved such that one vertex is at the origin $\mathbf{O} = (0, 0)^T$. We denote this translated element by q . The constant $C(\Omega^{(i)}) = C(q)$ depends only on the size and the shape of q and not on the position of $\Omega^{(i)}$ within the mesh. Moreover, it depends continuously on the position of the vertices of q , since the definition of the projector depends continuously on the vertices. Since the set of all shape regular triangles and quadrilaterals q which contain the origin in their boundary and have fixed size $\theta = \text{diam}(q)$ is compact, the maximum of $C(q)$ over all shape regular q of size θ exists and is attained for some triangle or quadrilateral q' , i.e.,

$$\max_{q \in E_{\rho, \theta}} C(q) = C(q') =: \sigma$$

for

$$E_{\rho, \theta} = \{q \subseteq \mathbb{R}^2 : \mathbf{O} \in \partial q, q \text{ is a shape regular triangle or quadrilateral with constant } \rho \text{ and } \text{diam}(q) = \theta\}.$$

By construction, σ depends only on ρ and θ and on the degree p , which we have assumed to be fixed. This completes the proof. \square

We can now prove approximation error bounds in standard Sobolev norms.

Theorem 2. *Let the mesh on Ω be shape regular and let $\Omega^{(i)}$ be an element of the mesh, let ℓ and m be integers, with $0 \leq \ell \leq 2$ and $4 \leq m \leq p+1$, and let the projector $\Pi_p^{(i)}$ be defined as in (38). There exists a constant $C > 0$ such that we have for all $\varphi \in H^m(\Omega^{(i)})$*

$$\left| \varphi - \Pi_p^{(i)} \varphi \right|_{H^\ell(\Omega^{(i)})} \leq C h_i^{m-\ell} |\varphi|_{H^m(\Omega^{(i)})},$$

where $h_i = \text{diam}(\Omega^{(i)})$. The constant C depends on the shape regularity parameter ρ and on p . We moreover have

$$\left\| \varphi - \Pi_p^{(i)} \varphi \right\|_{L^\infty(\Omega^{(i)})} \leq C h_i^m |\varphi|_{W^{m,\infty}(\Omega^{(i)})}$$

for all $\varphi \in W^{m,\infty}(\Omega^{(i)})$, where $|\cdot|_{W^{m,\infty}(D)}$ takes the essential supremum of all derivatives of order m over D .

Proof. The proof follows the proof of [8, Theorem 4.4.4] and [33, Theorem 4.6]. Let, for now, $h_i = 1$. Then we have the following

$$\left| \varphi - \Pi_p^{(i)} \varphi \right|_{H^\ell(\Omega^{(i)})} \leq \left\| \varphi - \Pi_p^{(i)} \varphi \right\|_{H^\ell(\Omega^{(i)})} \leq \|\varphi - \psi_p\|_{H^\ell(\Omega^{(i)})} + \left\| \psi_p - \Pi_p^{(i)} \varphi \right\|_{H^\ell(\Omega^{(i)})}$$

for any $\psi_p \in \mathbb{P}_p^2$. Due to Lemma 3 we have $\psi_p - \Pi_p^{(i)} \varphi = \Pi_p^{(i)}(\psi_p - \varphi)$. Hence, Lemma 4 yields for $\ell \leq 2$

$$\left\| \psi_p - \Pi_p^{(i)} \varphi \right\|_{H^\ell(\Omega^{(i)})} = \left\| \Pi_p^{(i)}(\psi_p - \varphi) \right\|_{H^\ell(\Omega^{(i)})} \leq \sigma \|\psi_p - \varphi\|_{C^2(\overline{\Omega^{(i)}})}.$$

A standard Sobolev inequality [8, Lemma 4.3.4] gives the bound

$$\|\psi_p - \varphi\|_{C^2(\overline{\Omega^{(i)}})} \leq C_{SI} \|\psi_p - \varphi\|_{H^4(\Omega^{(i)})},$$

where C_{SI} depends only on the shape regularity parameter ρ . Altogether we obtain

$$\left| \varphi - \Pi_p^{(i)} \varphi \right|_{H^\ell(\Omega^{(i)})} \leq (1 + \sigma C_{SI}) \inf_{\psi_p \in \mathbb{P}_p^2} \|\psi_p - \varphi\|_{H^4(\Omega^{(i)})} \leq C |\varphi|_{H^m(\Omega^{(i)})},$$

with $C = (1 + \sigma C_{SI}) C_{BH}$, where the last bound, for $4 \leq m \leq p+1$, comes from a Bramble-Hilbert estimate, with constant C_{BH} , as in [8, Lemma 4.3.8]. The dependence on the diameter h_i of the element $\Omega^{(i)}$ follows from a standard homogeneity argument. The estimate for

$$\left\| \varphi - \Pi_p^{(i)} \varphi \right\|_{L^\infty(\Omega^{(i)})}$$

follows similar steps as the H^ℓ -estimate and is omitted here. \square

From this local error estimate one can easily derive the following global estimate.

Corollary 2. *We assume to have a shape-regular, mixed mesh on Ω . Let ℓ and m be integers, with $0 \leq \ell \leq 2$ and $4 \leq m \leq p+1$. There exists a constant $C > 0$, depending on the degree p and on the shape regularity constant C_{SR} , such that we have for all $\varphi \in H^m(\Omega)$*

$$|\varphi - \Pi_p \varphi|_{H^\ell(\Omega)} \leq C h^{m-\ell} |\varphi|_{H^m(\Omega)},$$

as well as for all $\varphi \in W^{m,\infty}(\Omega)$

$$\|\varphi - \Pi_p \varphi\|_{L^\infty(\Omega)} \leq C h^m |\varphi|_{W^{m,\infty}(\Omega)}.$$

Here the projector Π_p is defined as in (37) and h denotes the length of the longest edge of the mesh.

Examples of interpolants $\Pi_p f$ together with numerical observation of the approximation order are provided in the next section.

5. Numerical examples

This section provides some numerical examples that confirm the derived theoretical results. In particular, the super-smooth C^1 Argyris-like space \mathcal{A}_p is employed for three different applications on several mixed triangle and quadrilateral meshes. The first two applications are the interpolation of a given function, based on the projection operator Π_p , and the L^2 -approximation. Both applications numerically verify the optimal approximation properties of the Argyris-like space \mathcal{A}_p . Thirdly, we solve a particular fourth order PDE given by the biharmonic equation, which requires the use of globally C^1 functions for solving the PDE via its weak form and Galerkin discretization.

5.1. Mixed meshes, refinement strategy & super-smooth C^1 spline spaces

We consider the three mixed triangle and quadrilateral meshes shown in Fig. 9–11 (first column) denoted by Mesh 1–3. The three mixed meshes are refined by splitting each triangle and each quadrilateral of the corresponding mesh into four triangles and into four quadrilaterals, respectively, as visualized in Fig. 12. As an example, the resulting refined meshes for the third level of refinement (i.e. for Level 3) are presented in Fig. 9–11 (second column). We further construct for all three meshes Argyris-like spaces \mathcal{A}_p as described in the previous section for the levels of refinement $L = 0, 1, \dots, 5$, and denote the resulting super-smooth C^1 spline spaces by $\mathcal{A}_{p,h}$, where $h = \mathcal{O}(2^{-L})$ is the length of the longest edge in the mesh.

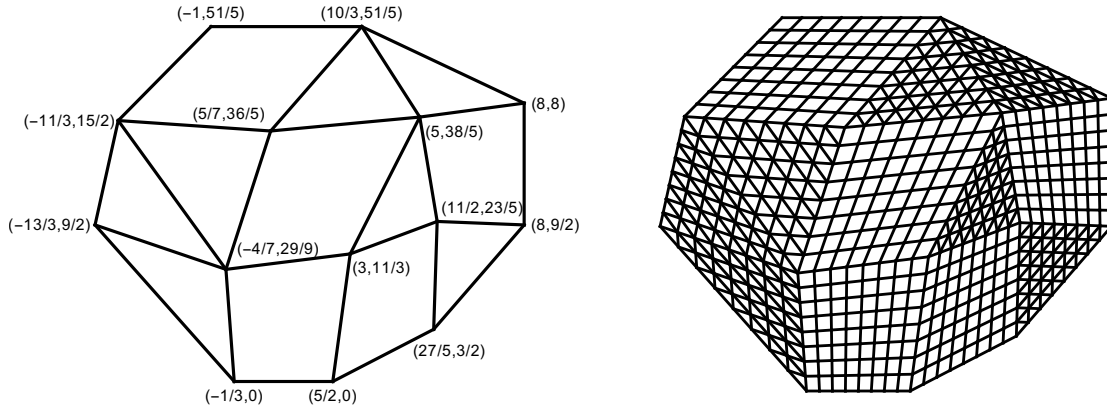


Figure 9: Mesh 1 – mixed triangle and quadrilateral mesh for the initial level of refinement (i.e. Level 0) with the coordinates of the vertices and for the third level of refinement (i.e. Level 3).

5.2. Interpolation

To test the interpolation error we choose a smooth function

$$f(\mathbf{x}) = f(x, y) = 4 \cos\left(\frac{2x}{3}\right) \sin\left(\frac{2y}{3}\right) \quad (39)$$

and compute the interpolants $\Pi_p f$ for degrees $p = 5, 6, \dots, 10$ on mixed meshes Mesh 1–3. Fig. 13 schematically presents the interpolation data we have used for degrees $p = 8$ and $p = 9$ when constructing interpolants over Mesh 1. Interpolating splines $\Pi_6 f$ over all three meshes are shown in Fig. 14. To compare between interpolants of different degrees we use the L^∞ -error $\|f - \Pi_p f\|_\infty$, which we compute numerically by evaluating in $51^2 = 2601$ and $\binom{52}{2} = 1326$ uniformly spaced points on every quadrilateral and triangle respectively. The errors for degrees $p = 5, 6, \dots, 10$ for all three meshes are given in Table 1.

Further, to numerically observe the approximation order, we compute interpolants $\Pi_p f$ over meshes with different refinement levels. Let us denote the L^∞ -error of the interpolant of degree p on level L by $\text{err}_{p,L}$. For Mesh 1, these values are shown in Table 2 together with the estimated decay exponents $\gamma_{p,L}$. The values in Table 2 numerically confirm that the approximation order for splines of degree p is optimal, i.e. $p + 1$.

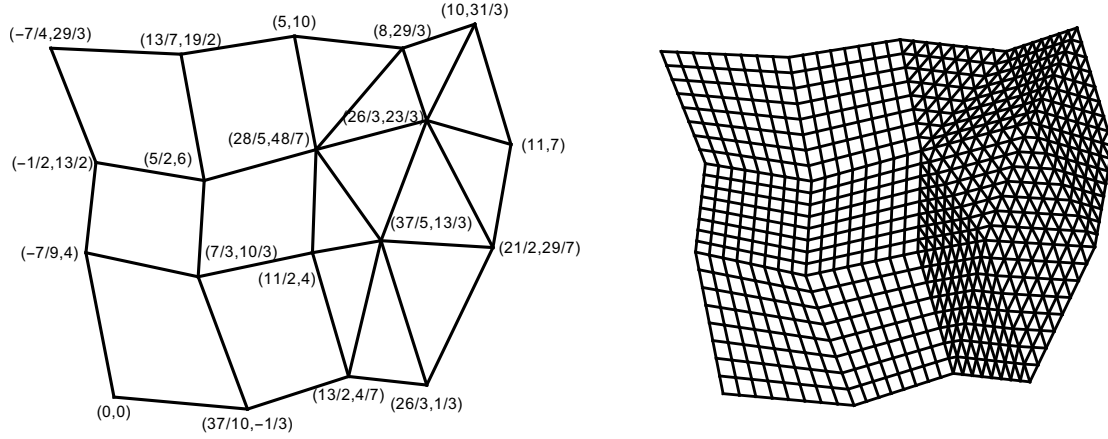


Figure 10: Mesh 2 – mixed triangle and quadrilateral mesh for the initial level of refinement with the coordinates of the vertices and for the third level of refinement.

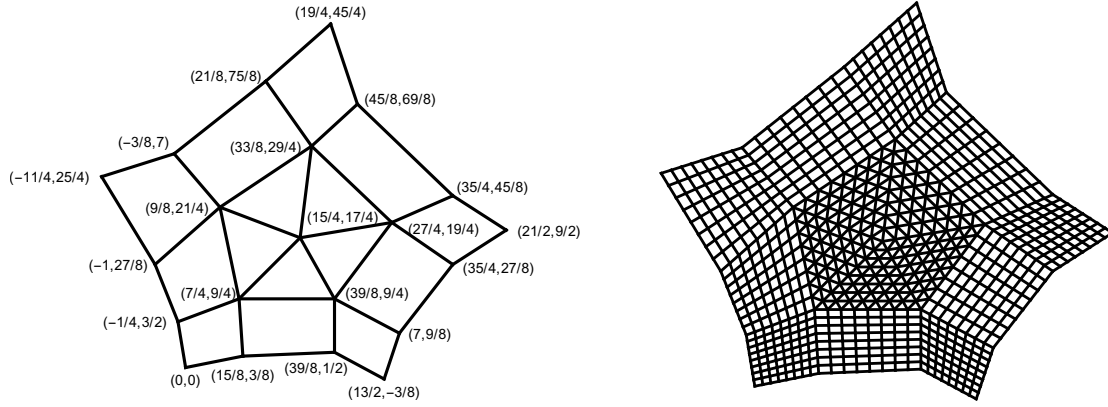


Figure 11: Mesh 3 – mixed triangle and quadrilateral mesh for the initial level of refinement with the coordinates of the vertices and for the third level of refinement.

Similar results hold true for the other two example meshes as one can see in Fig. 15, where the errors of interpolants of different degrees over different refinement levels are plotted in log–log-scale in dependence on the number of degrees of freedom.

5.3. L^2 -approximation

We use the constructed super-smooth C^1 spline spaces $\mathcal{A}_{5,h}$ to approximate in a least-squares sense the function (39) on meshes Mesh 1–3. That is, we compute in each case that function $f_h \in \mathcal{A}_{5,h}$, which minimizes the objective function

$$\int_{\Omega} (f_h(\mathbf{x}) - f(\mathbf{x}))^2 d\mathbf{x}.$$

Fig. 16 (second row) reports the resulting L^∞ -errors as well as the resulting L^2 -errors for different levels of refinement with respect to the number of degrees of freedom (NDOF). The obtained results indicate that both errors decrease with rates of optimal order of $\mathcal{O}(h^6)$, which numerically verify the optimal approximation power of the super-smooth C^1 Argyris-like space \mathcal{A}_5 .

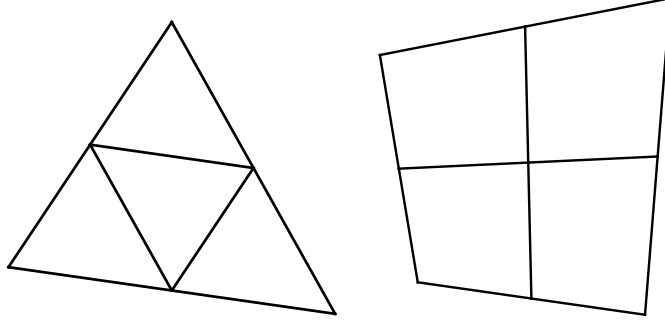


Figure 12: Each triangle (left) and each quadrilateral (right) is split as shown into four triangles and into four quadrilaterals, respectively.

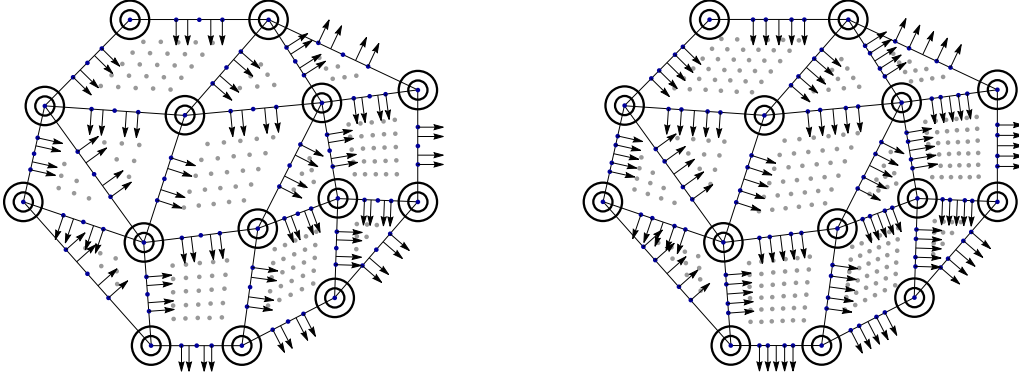


Figure 13: Schematic interpretation of interpolating data on Mesh 1 for degrees $p = 8$ (left) and $p = 9$ (right).

5.4. Solving the biharmonic equation

We solve a particular fourth order PDE, namely the biharmonic equation

$$\begin{cases} \Delta^2 u(\mathbf{x}) = g(\mathbf{x}) & \mathbf{x} \in \Omega \\ u(\mathbf{x}) = g_1(\mathbf{x}) & \mathbf{x} \in \partial\Omega \\ \frac{\partial u}{\partial \mathbf{n}}(\mathbf{x}) = g_2(\mathbf{x}) & \mathbf{x} \in \partial\Omega \end{cases} \quad (40)$$

on the Meshes 1–3 by employing the super-smooth C^1 spline spaces $\mathcal{A}_{5,h}$ as discretization spaces. For all three meshes, the functions g , g_1 and g_2 are derived from the same exact solution (39) as before for the case of L^2 -approximation. The biharmonic equation (40) is solved via its weak form and Galerkin projection by at first strongly imposing the Dirichlet boundary conditions to the numerical solution $u_h \in \mathcal{A}_{5,h}$. Let $\hat{\mathcal{A}}_{5,h}$

degree p	Mesh 1	Mesh 2	Mesh 3
5	$4.22291 \cdot 10^{-1}$	$1.01635 \cdot 10^{-1}$	$3.17295 \cdot 10^{-2}$
6	$9.72889 \cdot 10^{-2}$	$3.98448 \cdot 10^{-3}$	$1.16293 \cdot 10^{-2}$
7	$4.65926 \cdot 10^{-3}$	$6.25145 \cdot 10^{-4}$	$1.91039 \cdot 10^{-4}$
8	$1.99952 \cdot 10^{-3}$	$3.25673 \cdot 10^{-5}$	$1.17307 \cdot 10^{-4}$
9	$8.47799 \cdot 10^{-5}$	$6.50782 \cdot 10^{-6}$	$2.27334 \cdot 10^{-6}$
10	$4.27483 \cdot 10^{-5}$	$2.77481 \cdot 10^{-7}$	$1.27041 \cdot 10^{-6}$

Table 1: Table of errors $\|f - \Pi_p f\|_\infty$ of interpolants of different degrees over meshes Mesh 1–3.

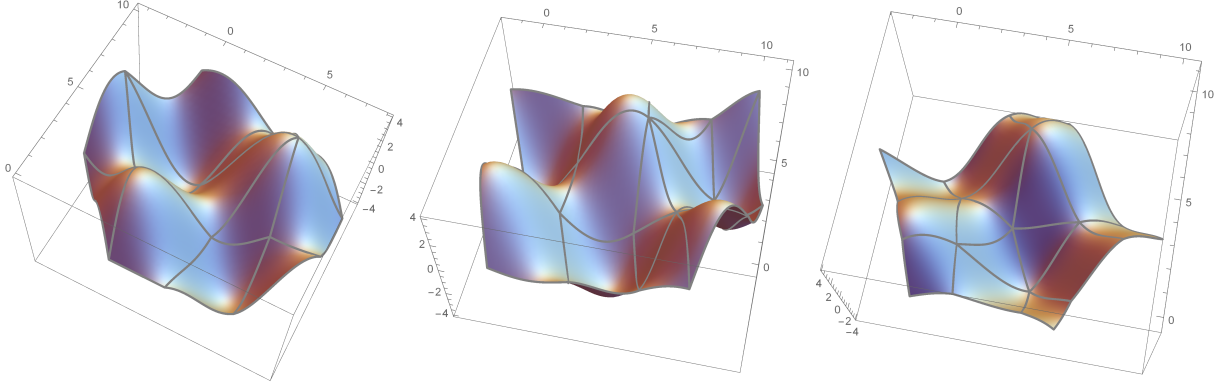


Figure 14: Interpolating splines $\Pi_6 f$ for the function (39) over three meshes Mesh 1–3.

	$p = 5$		$p = 6$		$p = 7$	
level L	error $\text{err}_{5,L}$	$\gamma_{5,L}$	error $\text{err}_{6,L}$	$\gamma_{6,L}$	error $\text{err}_{7,L}$	$\gamma_{7,L}$
level 0	$4.22291 \cdot 10^{-1}$	/	$9.72889 \cdot 10^{-2}$	/	$4.65926 \cdot 10^{-3}$	/
level 1	$2.00986 \cdot 10^{-2}$	4.39307	$9.50777 \cdot 10^{-4}$	6.67702	$6.53520 \cdot 10^{-5}$	6.15573
level 2	$3.40837 \cdot 10^{-4}$	5.88187	$8.10833 \cdot 10^{-6}$	6.87356	$2.69193 \cdot 10^{-7}$	7.92345
level 3	$5.44531 \cdot 10^{-6}$	5.96792	$6.54896 \cdot 10^{-8}$	6.95199	$1.06583 \cdot 10^{-9}$	7.98052
	$p = 8$		$p = 9$		$p = 10$	
level L	error $\text{err}_{8,L}$	$\gamma_{8,L}$	error $\text{err}_{9,L}$	$\gamma_{9,L}$	error $\text{err}_{10,L}$	$\gamma_{10,L}$
level 0	$1.99952 \cdot 10^{-3}$	/	$8.47799 \cdot 10^{-5}$	/	$4.27483 \cdot 10^{-5}$	/
level 1	$4.54388 \cdot 10^{-6}$	8.78151	$3.68637 \cdot 10^{-7}$	7.84538	$2.32038 \cdot 10^{-8}$	10.84729
level 2	$9.46490 \cdot 10^{-9}$	8.90712	$3.74188 \cdot 10^{-10}$	9.94423	$1.19579 \cdot 10^{-11}$	10.92218
level 3	$1.89790 \cdot 10^{-11}$	8.96204	$3.69027 \cdot 10^{-13}$	9.98582	$5.97942 \cdot 10^{-15}$	10.96567

Table 2: Table of L^∞ -errors for interpolants of different degrees p over Mesh 1 with different levels of refinement L together with estimates $\gamma_{p,L}$ of the decay exponent.

and $\tilde{\mathcal{A}}_{5,h}$ be the two isogeometric spline spaces defined via

$$\hat{\mathcal{A}}_{5,h} = \left\{ \varphi \in \mathcal{A}_{5,h} : \varphi(\mathbf{x}) = \frac{\partial \varphi}{\partial \mathbf{n}}(\mathbf{x}) = 0, \mathbf{x} \in \partial\Omega \right\}$$

and

$$\mathcal{A}_{5,h} = \hat{\mathcal{A}}_{5,h} \oplus \tilde{\mathcal{A}}_{5,h},$$

respectively. We aim at finding for the biharmonic equation (40) an approximated solution $u_h = \hat{u}_h + \tilde{u}_h$ with $\hat{u}_h \in \hat{\mathcal{A}}_{5,h}$ and $\tilde{u}_h \in \tilde{\mathcal{A}}_{5,h}$, where \tilde{u}_h is at first computed via L^2 -projection to approximately satisfy the Dirichlet boundary conditions, and is then used to find \hat{u}_h by solving the problem

$$\int_{\Omega} \Delta \hat{u}_h(\mathbf{x}) \Delta \hat{v}_h(\mathbf{x}) d\mathbf{x} = \int_{\Omega} g(\mathbf{x}) \hat{v}_h(\mathbf{x}) d\mathbf{x} - \int_{\Omega} \Delta \tilde{u}_h(\mathbf{x}) \Delta \hat{v}_h(\mathbf{x}) d\mathbf{x} \quad (41)$$

for all $\hat{v}_h \in \hat{\mathcal{A}}_{5,h}$. An isogeometric formulation of the problem (41) can be found e.g. in [2, 34].

The resulting relative L^2 -, H^1 - and H^2 -errors for the different levels of refinement, again with respect to the number of degrees of freedom, are shown in Fig. 16 (third row). The estimated convergence rates are for all examples of optimal order of $\mathcal{O}(h^6)$, $\mathcal{O}(h^5)$ and $\mathcal{O}(h^4)$ with respect to the L^2 -, H^1 - and H^2 -norm, respectively.

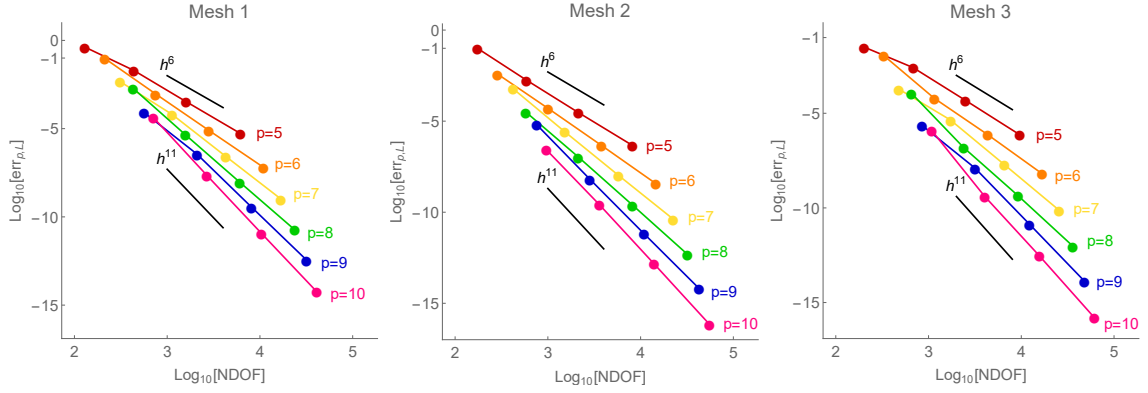


Figure 15: L^∞ -errors of interpolants of different degrees p over meshes Mesh 1–3 with different refinement levels. Errors are shown in log–log-scale in dependence on the number of degrees of freedom.

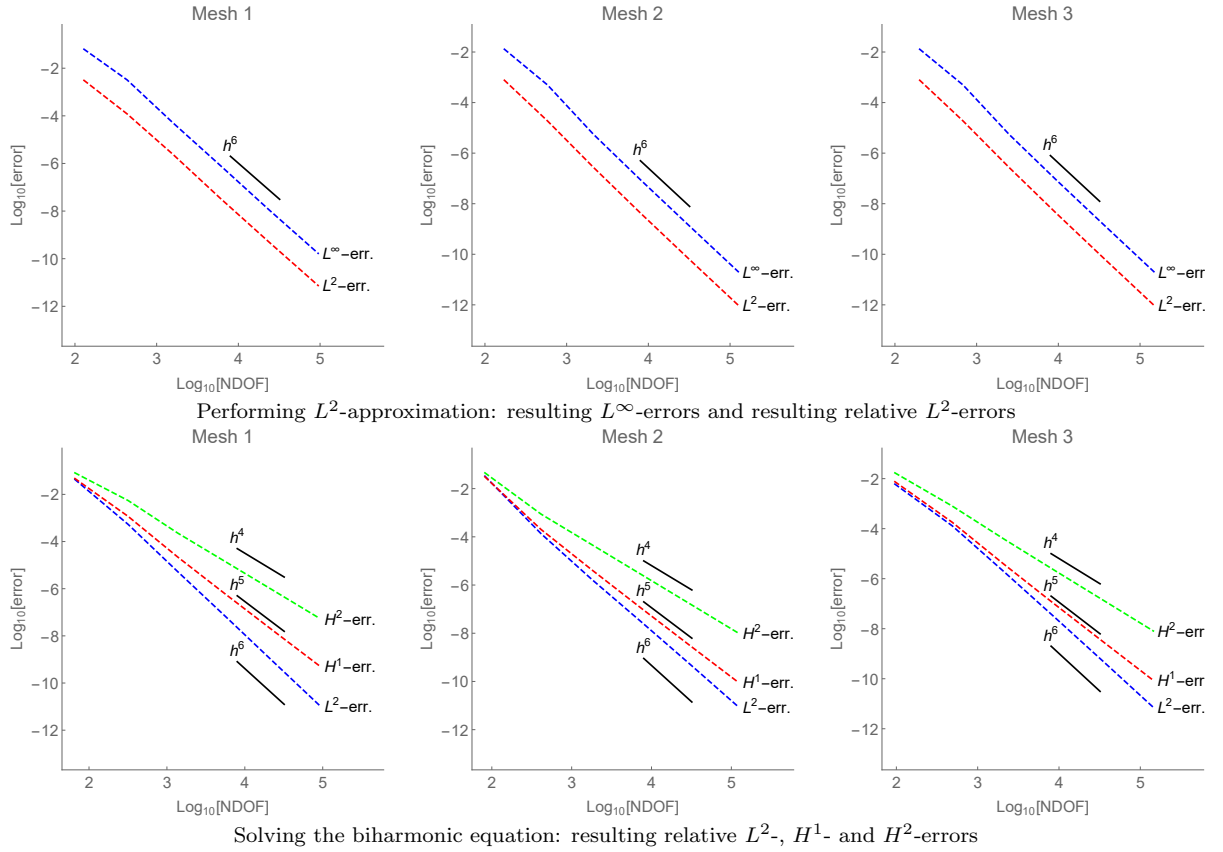


Figure 16: Performing L^2 -approximation and solving the biharmonic equations for the exact solutions (39) on the Meshes 1–3 from Fig. 9–11 and the resulting errors.

6. Conclusions

We studied a construction of C^1 splines over mixed triangle and quadrilateral meshes for polynomial degrees $p \geq 5$. The degrees of freedom are given by C^2 -data at the vertices, point data and normal derivative data at suitable points along the edges as well as additional point data in the interior of the elements. The resulting space is C^1 globally and C^2 at all vertices. The degrees of freedom define a stable projection operator which, together with the local polynomial reproduction, yields optimal approximation error bounds with respect to the mesh size for L^∞ , L^2 as well as Sobolev norms H^1 and H^2 .

In this paper we only considered planar (bi)linear elements. Extensions to domains with curved boundaries or to surface domains were already discussed separately in case of quadrilateral meshes as well as triangle meshes. For quadrilateral meshes, [4, 39] provided extensions to elements with curved boundaries, i.e. elements where one boundary edge is curved and the other three are straight. Extensions to surface domains were briefly discussed for spline patches in [15, 30]. Constructions of C^1 surfaces of arbitrary topology using triangle meshes were developed in [21]. To extend the construction to mixed surface meshes and mixed meshes with curved boundaries is of vital interest for the applicability of the proposed elements in a general isogeometric framework based on CAD geometries. However, to work out the details of such extensions in the mixed case requires further studies which we intend to do in the future.

Acknowledgments

The authors wish to thank the anonymous reviewers for their comments that helped to improve the paper. This paper was developed within the Scientific and Technological Cooperation “Splines in Geometric Design and Numerical Analysis” between Austria and Slovenia 2018-19, funded by the OeAD under grant nr. SI 28/2018 and by ARRS bilateral project nr. BI-AT/18-19-012.

The research of M. Kapl is partially supported by the Austrian Science Fund (FWF) through the project P 33023. The research of T. Takacs is partially supported by the Austrian Science Fund (FWF) and the government of Upper Austria through the project P 30926-NBL. The research of M. Knez is partially supported by the research program P1-0288 and the research project J1-9104 from ARRS, Republic of Slovenia. The research of J. Grošelj is partially supported by the research program P1-0294 from ARRS, Republic of Slovenia. The research of V. Vitrih is partially supported by the research program P1-0404 from ARRS, Republic of Slovenia. This support is gratefully acknowledged.

References

- [1] J. H. Argyris, I. Fried, and D. W. Scharpf. The TUBA family of plate elements for the matrix displacement method. *The Aeronautical Journal*, 72(692):701–709, 1968.
- [2] A. Bartezzaghi, L. Dedè, and A. Quarteroni. Isogeometric analysis of high order partial differential equations on surfaces. *Comput. Methods Appl. Mech. Engrg.*, 295:446 – 469, 2015.
- [3] Y. Bazilevs, V. M. Calo, T. J. R. Hughes, and Y. Zhang. Isogeometric fluid-structure interaction: theory, algorithms, and computations. *Computational mechanics*, 43(1):3–37, 2008.
- [4] M. Bercovier and T. Matskewich. *Smooth Bézier Surfaces over Unstructured Quadrilateral Meshes*. Lecture Notes of the Unione Matematica Italiana, Springer, 2017.
- [5] A. Blidia, B. Mourrain, and N. Villamizar. G^1 -smooth splines on quad meshes with 4-split macro-patch elements. *Computer Aided Geometric Design*, 52–53:106–125, 2017.
- [6] A. Blidia, B. Mourrain, and G. Xu. Geometrically smooth spline bases for data fitting and simulation. *Computer Aided Geometric Design*, 78:101814, 2020.
- [7] F. K. Bogner, R. L. Fox, and L. A. Schmit. The generation of interelement compatible stiffness and mass matrices by the use of interpolation formulae. In *Proc. Conf. Matrix Methods in Struct. Mech., AirForce Inst. of Tech., Wright Patterson AF Base, Ohio*, 1965.
- [8] S. C. Brenner and R. Scott. *The Mathematical Theory of Finite Element Methods*, volume 15. Springer Science & Business Media, 2007.
- [9] S. C. Brenner and L.-Y. Sung. C^0 interior penalty methods for fourth order elliptic boundary value problems on polygonal domains. *Journal of Scientific Computing*, 22(1-3):83–118, 2005.
- [10] F. Buchegger, B. Jüttler, and A. Mantzaflaris. Adaptively refined multi-patch B-splines with enhanced smoothness. *Applied Mathematics and Computation*, 272:159 – 172, 2016.
- [11] C.L. Chan, C. Anitescu, and T. Rabczuk. Isogeometric analysis with strong multipatch C^1 -coupling. *Comput. Aided Geom. Design*, 62:294–310, 2018.

- [12] C. K. Chui and T. X. He. On the dimension of bivariate superspline spaces. *Mathematics of Computation*, 53(187):219–234, 1989.
- [13] P. G. Ciarlet. *The Finite Element Method for Elliptic Problems*, volume 40. Siam, 2002.
- [14] F. Cirak, M. Ortiz, and P. Schröder. Subdivision surfaces: a new paradigm for thin-shell finite-element analysis. *Int. J. Numer. Meth. Engng*, 47(12):2039–2072, 2000.
- [15] A. Collin, G. Sangalli, and T. Takacs. Analysis-suitable G^1 multi-patch parametrizations for C^1 isogeometric spaces. *Computer Aided Geometric Design*, 47:93 – 113, 2016.
- [16] P. Dierckx. On calculating normalized Powell-Sabin B-splines. *Computer Aided Geometric Design*, 15(1):61–78, 1997.
- [17] H. Gómez, V. M. Calo, Y. Bazilevs, and T. J.R. Hughes. Isogeometric analysis of the Cahn–Hilliard phase-field model. *Comput. Methods Appl. Mech. Engrg.*, 197(49):4333–4352, 2008.
- [18] H. Gómez, T. J.R. Hughes, X. Nogueira, and V. M. Calo. Isogeometric analysis of the isothermal Navier–Stokes–Korteweg equations. *Comput. Methods Appl. Mech. Engrg.*, 199(25):1828–1840, 2010.
- [19] J. A. Gregory and J. M. Hahn. Geometric continuity and convex combination patches. *Comput. Aided Geom. Design*, 4(1-2):79–89, 1987.
- [20] D. Groisser and J. Peters. Matched G^k -constructions always yield C^k -continuous isogeometric elements. *Computer Aided Geometric Design*, 34:67 – 72, 2015.
- [21] S. Hahmann and G.-P. Bonneau. Triangular G^1 interpolation by 4-splitting domain triangles. *Computer Aided Geometric Design*, 17:731–757, 2000.
- [22] S.-M. Hu. Conversion between triangular and rectangular Bézier patches. *Computer Aided Geometric Design*, 18(7):667–671, 2001.
- [23] T. J. R. Hughes, J. A. Cottrell, and Y. Bazilevs. Isogeometric analysis: CAD, finite elements, NURBS, exact geometry and mesh refinement. *Comput. Methods Appl. Mech. Engrg.*, 194(39-41):4135–4195, 2005.
- [24] G. Jaklič and T. Kanduč. Hermite parametric surface interpolation based on Argyris element. *Computer Aided Geometric Design*, 56:67–81, 2017.
- [25] N. Jaxon and X. Qian. Isogeometric analysis on triangulations. *Computer-Aided Design*, 46:45–57, 2014.
- [26] B. Jüttler, A. Mantzaflaris, R. Perl, and M. Rumpf. On numerical integration in isogeometric subdivision methods for PDEs on surfaces. *Comput. Methods Appl. Mech. Engrg.*, 302:131–146, 2016.
- [27] M. Kapl, F. Buchegger, M. Bercovier, and B. Jüttler. Isogeometric analysis with geometrically continuous functions on planar multi-patch geometries. *Comput. Methods Appl. Mech. Engrg.*, 316:209 – 234, 2017.
- [28] M. Kapl, M. Byrtus, and B. Jüttler. Triangular bubble spline surfaces. *Computer-Aided Design*, 43(11):1341 – 1349, 2011.
- [29] M. Kapl, G. Sangalli, and T. Takacs. Dimension and basis construction for analysis-suitable G^1 two-patch parameterizations. *Computer Aided Geometric Design*, 52–53:75 – 89, 2017.
- [30] M. Kapl, G. Sangalli, and T. Takacs. Construction of analysis-suitable G^1 planar multi-patch parameterizations. *Computer-Aided Design*, 97:41 – 55, 2018.
- [31] M. Kapl, G. Sangalli, and T. Takacs. Isogeometric analysis with C^1 functions on planar, unstructured quadrilateral meshes. *The SMAI Journal of Computational Mathematics*, S5:67–86, 2019.
- [32] M. Kapl, G. Sangalli, and T. Takacs. An isogeometric C^1 subspace on unstructured multi-patch planar domains. *Computer Aided Geometric Design*, 69:55–75, 2019.
- [33] M. Kapl, G. Sangalli, and T. Takacs. A family of C^1 quadrilateral finite elements. *arXiv preprint arXiv:2005.04251*, 2020.
- [34] M. Kapl, V. Vitrih, B. Jüttler, and K. Birner. Isogeometric analysis with geometrically continuous functions on two-patch geometries. *Comput. Math. Appl.*, 70(7):1518 – 1538, 2015.
- [35] J. Kiendl, Y. Bazilevs, M.-C. Hsu, R. Wüchner, and K.-U. Bletzinger. The bending strip method for isogeometric analysis of Kirchhoff-Love shell structures comprised of multiple patches. *Comput. Methods Appl. Mech. Engrg.*, 199(35):2403–2416, 2010.
- [36] J. Kiendl, K.-U. Bletzinger, J. Linhard, and R. Wüchner. Isogeometric shell analysis with Kirchhoff-Love elements. *Comput. Methods Appl. Mech. Engrg.*, 198(49):3902–3914, 2009.
- [37] H.-J. Kim, Y.-D. Seo, and S.-K. Youn. Isogeometric analysis for trimmed CAD surfaces. *Computer Methods in Applied Mechanics and Engineering*, 198(37-40):2982–2995, 2009.
- [38] M.-J. Lai and L. L. Schumaker. *Spline functions on triangulations*. Cambridge University Press, 2007.
- [39] T. Matskewich. *Construction of C^1 surfaces by assembly of quadrilateral patches under arbitrary mesh topology*. PhD thesis, Hebrew University of Jerusalem, 2001.
- [40] B. Mourrain, R. Vidunas, and N. Villamizar. Dimension and bases for geometrically continuous splines on surfaces of arbitrary topology. *Computer Aided Geometric Design*, 45:108 – 133, 2016.
- [41] T. Nguyen, K. Karčiauskas, and J. Peters. A comparative study of several classical, discrete differential and isogeometric methods for solving poisson’s equation on the disk. *Axioms*, 3(2):280–299, 2014.
- [42] T. Nguyen and J. Peters. Refinable C^1 spline elements for irregular quad layout. *Computer Aided Geometric Design*, 43:123 – 130, 2016.
- [43] J. Peters. Smooth mesh interpolation with cubic patches. *Computer-Aided Design*, 22(2):109 – 120, 1990.
- [44] J. Peters. C^1 -surface splines. *SIAM Journal on Numerical Analysis*, 32(2):645–666, 1995.
- [45] J. Peters. Geometric continuity. In *Handbook of computer aided geometric design*, pages 193–227. North-Holland, Amsterdam, 2002.
- [46] J. Peters and U. Reif. *Subdivision surfaces*, volume 3 of *Geometry and Computing*. Springer-Verlag, Berlin, 2008.
- [47] U. Reif. Biquadratic G-spline surfaces. *Comput. Aided Geom. Des.*, 12(2):193–205, 1995.
- [48] A. Riffnaller-Schiefer, U. H. Augsdörfer, and D. W. Fellner. Isogeometric shell analysis with NURBS compatible subdivision surfaces. *Applied Mathematics and Computation*, 272:139–147, 2016.

- [49] G. Sangalli, T. Takacs, and R. Vázquez. Unstructured spline spaces for isogeometric analysis based on spline manifolds. *Computer Aided Geometric Design*, 47:61–82, 2016.
- [50] F. Scholz, A. Mantzaflaris, and B. Jüttler. First order error correction for trimmed quadrature in isogeometric analysis. In *Chemnitz Fine Element Symposium*, pages 297–321. Springer, 2017.
- [51] Y. Song and E. Cohen. Volume completion for trimmed B-reps. In *2019 23rd International Conference in Information Visualization–Part II*, pages 147–155. IEEE, 2019.
- [52] H. Speleers. Construction of normalized B-splines for a family of smooth spline spaces over Powell–Sabin triangulations. *Constructive Approximation*, 37(1):41–72, 2013.
- [53] H. Speleers, C. Manni, F. Pelosi, and M. L. Sampoli. Isogeometric analysis with Powell–Sabin splines for advection–diffusion–reaction problems. *Computer methods in applied mechanics and engineering*, 221:132–148, 2012.
- [54] A. Tagliabue, L. Dedè, and A. Quarteroni. Isogeometric analysis and error estimates for high order partial differential equations in fluid dynamics. *Computers & Fluids*, 102:277 – 303, 2014.
- [55] T. Takacs. Construction of smooth isogeometric function spaces on singularly parameterized domains. In *International Conference on Curves and Surfaces*, pages 433–451. Springer, 2014.
- [56] D. Toshniwal, H. Speleers, and T. J. R. Hughes. Smooth cubic spline spaces on unstructured quadrilateral meshes with particular emphasis on extraordinary points: Geometric design and isogeometric analysis considerations. *Comput. Methods Appl. Mech. Engrg.*, 327:411–458, 2017.
- [57] D. J. Walton and D. S. Meek. A triangular G^1 patch from boundary curves. *Computer-Aided Design*, 28(2):113–123, 1996.
- [58] Q. Zhang, M. Sabin, and F. Cirak. Subdivision surfaces with isogeometric analysis adapted refinement weights. *Computer-Aided Design*, 102:104–114, 2018.